Journal of Medicinal Chemistry

ARTICLE

pubs.acs.org/jmc

Designing Nonsaccharide, Allosteric Activators of Antithrombin for Accelerated Inhibition of Factor Xa

Rami A. Al-Horani, Aiye Liang, and Umesh R. Desai*

Department of Medicinal Chemistry and Institute for Structural Biology and Drug Discovery, Virginia Commonwealth University, Richmond, Virginia 23298, United States

ABSTRACT: Antithrombin is a key regulator of coagulation and prime target of heparins, clinically used anticoagulants. Heparins induce a two-step conformational activation of antithrombin, a process that has remained challenging to target with molecules devoid of the antithrombin-binding pentasaccharide DEFGH. Computational screening of a focused library led to the design of two tetra-sulfated *N*-arylacyl tetrahydroisoquinoline variants as potential nonsaccharide activators of antithrombin. A high yielding synthetic scheme based on Horner−Wadsworth−Emmons or Pictet−Spengler reactions was developed to facilitate the functionalization of the tetrahydoisoquinoline ring, which upon further amidation, deprotection, and sulfation gave the targeted nonsaccharide activators. Spectrofluorometric measurement of affinity displayed antithrombin binding affinities in the low to high micromolar range at pH 6.0, *I* 0.05, 25 °C. Measurement of second-order rate constants of antithrombin inhibition of factor Xa in the presence and absence of the designed activators showed antithrombin activation in the range of 8−80-fold in the pH 6.0 buffer. This work puts forward **20c**, a novel tetra-sulfated *N*-arylacyl tetrahydroisoquinoline-based molecule, that activates AT only 3.8-fold less than that achieved with DEFGH, suggesting a strong possibility of rationally designing sulfated organic molecules as clinically relevant AT activators.

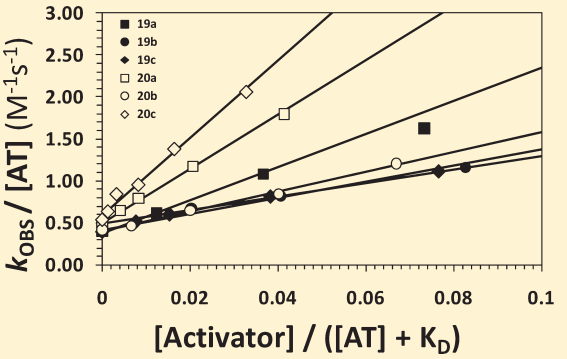

INTRODUCTION

Antithrombin (AT), a plasma glycoprotein belonging to the serpin superfamily of proteins, is a major inhibitor of coagulation enzymes, particularly factor Xa (fXa), factor IXa, and thrombin.[1,2] It performs this function under physiological conditions with the aid of heparin, a natural, highly sulfated polysaccharide, which accelerates the inhibitor's rate of reaction with fXa and other enzymes several hundred-fold.[3] A characteristic feature of this process is the allosteric, induced-fit mechanism of heparin activation of AT.[4−6] In this process, the first step is the recognition of the heparin binding site (HBS) in the serpin by heparin to form a low-affinity initial recognition complex, which is followed by a major conformational change in the main body of the protein (Figure 1A). Heparin drives the activation process forward because it greatly stabilizes the conformationally altered state of the inhibitor, called the activated form (AT*), which is much better recognized by fXa than the native form (AT). This classic induced-fit phenomenon is the fundamental basis for the use of heparin as an anticoagulant drug in the clinic.

The HBS in AT is a fairly large surface-exposed domain consisting of a large number of positively charged residues including Lys11, Arg13, Arg24, Arg46, Arg47, Lys114, Lys125, Arg129, Arg132, Lys133, and Lys136.[2,7] Full-length heparin (FLH) is thought to occupy the entire HBS. In contrast, a specific five-residue sequence, called the DEFGH sequence (Figure 1B), binds in the region formed by Lys114, Lys125, and Arg129, which is referred to as the pentasaccharide-binding site (PBS). Adjacent to the PBS is an electropositive domain formed by Arg132, Lys133, and Lys136, which engage the FLH chain and enhance its binding affinity relative to DEFGH.[8] This domain is called the extended heparin binding site (EHBS).

Detailed structure−activity studies have shown that the trisaccharide DEF sequence of the pentasaccharide DEFGH is critical for both steps of the induced-fit process, i.e., initial recognition as well as conformational activation.[5,6,9,10] Specifically, synthetic trisaccharide DEF was found to activate AT nearly 300-fold, equivalent to the acceleration achieved with the DEFGH, albeit with much lower affinity (66 μM at pH 7.4).[5,9] Mechanistically, DEF utilizes the induced-fit pathway to activate AT. Yet, select variants of DEFGH that do not utilize the induced-fit pathway are also known. These activators, e.g., tetrasaccharide EFGH, utilize the pre-equilibrium pathway (Figure 1A), an alternative activation mechanism of AT activation, which is also a two-step allosteric process relying on a pre-existing equilibrium to drive conformational activation.[5]

Clinically used FLH is a highly complex molecule known to be associated with multiple adverse effects including hemorrhage, thrombocytopenia, osteoporosis, and inconsistent patient response.[11] The animal origin of the drug is also a concern as implicated by recent incidences of contamination with oversulfated chondroitin sulfate.[12−14] A reduction in

Received: June 27, 2011
Published: July 29, 2011

dx.doi.org/10.1021/jm2008387 | *J. Med. Chem.* 2011, 54, 6125–6138

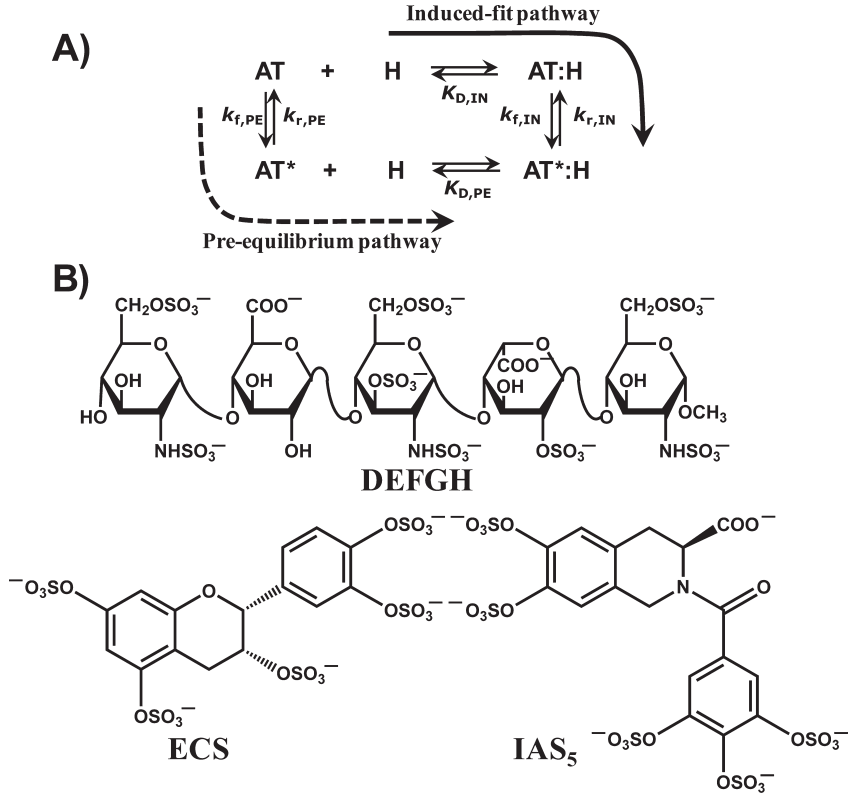

Figure 1. (A) Multistep mechanism of heparin activation of antithrombin. AT = native antithrombin; AT* = conformationally altered antithrombin; H = heparin. $K_{D,IN}$ and $K_{D,PE}$ refer to equilibrium dissociation constants of the first and last step of the induced-fit (IF) and pre-equilibrium (PE) pathways, respectively. k_f and k_r refer to forward and reverse rate constants in the two pathways. See text for additional details. (B) Structures of heparin pentasaccharide DEFGH, which is known to activate AT through the induced-fit mechanism, and nonsaccharide aromatic activators ECS and IAS_5, which are thought to activate AT through the pre-equilibrium mechanism.

molecular weight and polydispersity of FLH preparations as achieved in low-molecular-weight heparins (LMWHs) is known to reduce these adverse effects.

Structurally, the heparin-based anticoagulant therapy has remained essentially unchanged since its introduction in the 1930s. Despite its major success, heparins are beset with high bleeding risk.[11] In addition, the presence of a large number of negative charges on chains of FLH and LMWHs[3,15,16] induce significant nonspecific interactions with proteins of the plasma as well as membranes and possibly contribute to complications. A synthetic version of DEFGH, called fondaparinux (Figure 1B), is arguably the best anticoagulant with regard to such complications[17,18] but its synthesis is long-winding and expensive, while it too suffers from bleeding risks.[17−20]

Numerous attempts have been made to discover molecules that activate AT to overcome the drawbacks of heparins. A fundamental tenet of such efforts has been the assumed requirement of a saccharide scaffold.[21−27] Interestingly, comparative studies with a number of scaffolds such as Curdlan sulfate,[23] fucoidan,[21] galactomannan,[25] chitosan,[24] and others suggest that the heparin scaffold is uniquely tuned to activate AT. In fact, all newer molecules designed to potently bind AT have been derivatives of DEFGH.[2,10,28,29]

At a fundamental level, discovering AT activators unlike DEFGH and other heparins is challenging. No principles have been elucidated for designing highly sulfated molecules that allosterically activate a protein, such as antithrombin. The major difficulty in designing such allosteric activators is that the binding site is shallow and highly surface exposed, which tends to not subscribe to a high affinity interaction. In addition, activation requires that the binding energy is transmitted to the main body of the protein to induce activation. We had earlier utilized two independent approaches for designing AT activators that are radically different from the DEFGH-based saccharide molecules.[30,31] Our first-generation molecules, sulfated flavan-3-ols (Figure 1B), were designed using a computerized, structure-based design algorithm. Sulfated flavans-3-ols were the first designed aromatic AT activators that were radically different from heparins and attempted to functionally mimic trisaccharide DEF.[30,32,33] In the second approach, we utilized a pharmacophore-based approach of mimicking trisaccharide DEF function to design sulfated tetrahydroisoquinoline-3-carboxylic acids (THIQ3CA).[31] These studies led to the identification of IAS_5 (Figure 1B), a molecule that displayed AT activation of nearly 30-fold.

Our success with IAS_5 indicated a strong possibility of uncovering potent, ease-to-synthesize, small aromatic AT activators through a rational approach. Such nonsaccharide mimetics of heparin are likely to offer significant advantages such as superior nonionic binding energy in AT recognition,[32] greater hydrophobicity for possible oral bioavailability,[34−36] better synthetic accessibility, and narrower specificity of function in comparison to heparin's multitude of activities. Herein, we report our work with a focused library of tetra-sulfated *N*-arylacyl tetrahydroisoquinoline (THIQ) derivatives. Our work puts forward a novel sulfated aromatic molecule that exhibits ~80-

dx.doi.org/10.1021/jm2008387 |*J. Med. Chem.* 2011, 54, 6125–6138

fold activation of AT, which is only 3.8-fold less than that achieved with DEFGH. The level of AT activation induced by this third-generation molecule suggests that iterative rational design will lead to sulfated organic molecules as clinically relevant AT activators.

EXPERIMENTAL SECTION

Chemicals. Anhydrous CH_2Cl_2, THF, CH_3CN, and DMF were purchased from Sigma-Aldrich and used as such. All other solvents were of reagent gradient and used as purchased. Analytical TLC was performed using UNIPLATE silica gel GHLF 250 um precoated plates (ANALTECH, Newark, DE). TLC was visualized by electromagnetic wave of 254 nm and/or iodine. Column chromatography was performed using silica gel (200−400 mesh, 60 Å) from Sigma Aldrich. Chemical reactions sensitive to air or moisture were carried out under nitrogen atmosphere in oven-dried glassware. All reagent solutions unless otherwise noted were handled under an inert nitrogen atmosphere using syringe techniques.

Proteins. Human plasma AT and human fXa were purchased from Haematologic Technologies (Essex Junction, VT). Molar concentration of AT was calculated from absorbance measurements at 280 nm using a ε_{max} of 37700 M^{-1} cm^{-1}. AT was stored in 20 mM sodium phosphate buffer, pH 7.4, containing 100 mM NaCl, 0.1 mM EDTA, and 0.1% (w/v) PEG8000 at −78 °C, while fXa was stored in 5 mM MES buffer, pH 6.0, containing 25 mM NaCl at −78 °C. Spectrozyme FXa was obtained from American Diagnostics (Greenwich, CT) and prepared in 20 mM sodium phosphate buffer, pH 7.4, containing 100 mM NaCl, 0.1 mM EDTA, and 0.1% (w/v) PEG8000.

Modeling Antithrombin. Sybyl 8.1 (Tripos Associates, St. Louis, MO) was used for molecular modeling of AT−activator complexes. The structure of activated form of AT (ID: 2GD4) was acquired from the Protein Data Bank (www.rcsb.org). Chain I of the crystal structure, which corresponds to the inhibitory monomer, was used as a model of the activated antithrombin conformation. This form does not report the side chains of Arg46, Lys125, Arg132, Lys136, and Lys275, probably due to their significant flexibility. These side chains were introduced through appropriate modifications in Sybyl. Hydrogen atoms were added to the 2GD4 structure, while inorganic ions and water molecules were removed. Individual atoms were assigned Gasteiger−Hückel charges. To prepare this structure for docking and scoring protocols, energy minimization was performed using a Tripos force field so as to reach a terminating gradient of 0.5 kcal/mol $Å^2$ or a maximum of 100000 iterations.

Modeling the Virtual Library of Sulfated *N*-Arylacyl THIQ Derivatives. Ninety IAS_5-related potential AT activators were "synthesized" in silico using the LEGION combinatorial library design generator. For the sulfated activators, including IAS_5, that have carboxylic group at 3-position, both the enantiomers were modeled. The atom type of sulfur and oxygen atoms in sulfate groups was modified to S.o2 and O.co2, respectively, and an "aromatic" bond type was modeled between these atoms. The molecules were assigned Gasteiger−Hückel charges and were then energetically minimized using a Tripos force field until a terminating gradient of 0.5 kcal/mol $Å^2$ or a maximum of 100000 iterations.

Docking and Scoring. Docking of the potential sulfated AT activators onto the EHBS of the activated form of AT (AT*) was performed with GOLD 4.1 (Cambridge Crystallographic Data Center, UK). The EHBS comprised of electropositive residues, Arg129, Arg132, Lys133, Lys136, and Lys275 and other residues around them, as reported earlier.[2,8] GOLD is a "soft docking" method that implicitly handles local protein flexibility by allowing a small degree of interpenetration, or van der Waals overlap, of ligand and protein atoms. GOLD also optimizes the positions of hydrogen-bond donating atoms on Ser, Thr, Tyr, and most importantly, Lys and Arg residues as part of the docking process. Except for the automated number of iterations, the allowed amide bond flip and the prohibited early termination, default parameters were employed during the GOLD docking runs. Docking was driven by the GOLD scoring function, while for ranking the docked solutions, a linear, modified form of the same scoring function (eq 1) was used, as reported earlier.[37]

$$GOLD_{Score} = HB_{EXT} + 1.375 \times VDW_{EXT} \quad (1)$$

In this equation, HB_{EXT} and VDW_{EXT} are the "external" (nonbonded interactions taking place between the ligand and the target protein) hydrogen bonding and van der Waals terms, respectively.

In addition to GOLD score, Hydropathic INTeractions (HINT) (EduSoft LC, Ashland, VA) scoring function was also used to score AT−activator complexes. HINT scores each atom−atom interaction in the ligand−biomolecule complex using a parameter set derived from experimental solvation partition coefficients.[38] The interaction scores were calculated for each pose derived from docking using eq 2, which describes the overall interaction as a double sum over the atoms within each component.[30,32,37−39] In this equation, S is the solvent accessible surface area, a is the hydrophobic atom constant, T is a descriptor function (vide infra), and R and r are functions of the distance between atoms i and j. From this equation, a binding score is calculated where bij describes specific interaction between atoms i and j, and B describes the total interaction score between the two species.

$$B = \sum_{i=1}^{\text{atom}} \sum_{j=1}^{\text{atom}} b_{ij} = \sum\sum (S_i a_i S_j a_j R_{ij} T_{ij} + r_{ij}) \quad (2)$$

For HINT scoring of AT−activator complexes, energy minimization was first performed using Tripos force field until a terminating gradient of 0.005 kcal/mol $Å^2$ was reached. AT and the activator were then partitioned as distinct molecules. AT was assigned HINT parameters from a dictionary of previously determined values. "Essential" hydrogen atoms, i.e., only those attached to polar atoms, were explicitly considered in the models. Because HINT parameters for the sulfur atoms in higher oxidation states including sulfates are not well-established, sulfur interaction scores were removed from analysis.[30,32,40]

Chemical Characterization of Compounds. ^1H and ^{13}C NMR were recorded on Bruker-400 MHz spectrometer in either $CDCl_3$, CD_3OD, acetone-d_6, or D_2O. Signals, in part per million (ppm), are either relative to the internal standard (tetramethyl silane, TMS) or to the residual peak of the solvent. The NMR data are reported as chemical shift (ppm), multiplicity of signal (s = singlet, d = doublet, t = triplet, q = quartet, dd = doublet of doublet, m = multiplet), coupling constants (Hz), and integration. ESI MS of unsulfated molecules were recorded using Waters Acquity TQD MS spectrometer in positive ion mode. Samples were dissolved in methanol and infused at a rate of 20 μL/min. Mass scans were obtained in the range of 200−700 amu with a scan time of 1s and a scan rate of 500 amu/s. The capillary voltage was varied between 3 and 4 kV, while the cone voltage ranged from 38 to103 V. For sulfated molecules, ESI MS were recorded in negative ion mode. Samples were dissolved in 0.5% (v/v) formic acid in water and infused at a rate of 20 μL/min. Mass scans were obtained in the range of 200−1000 amu with a scan time of 1s and a scan rate of 800 amu/s. The capillary voltage was varied between 2.2 and 3.9 kV, while the cone voltage ranged from 60 to 74 V. Ionization conditions were optimized for each compound to maximize the ionization of the parent ion. Generally, the extractor voltage was set to 3 V, the Rf lens voltage was 0.1 V, the source block temperature was set to 150 °C, and the desolvation temperature was about 250 °C.

Purification and Analytical Identification of Sulfated Compounds. Sulfated nonsaccharide activators were purified using Sephadex G10 size exclusion chromatography. The quarternary ammonium counterion of sulfate groups present in the activators were exchanged

for sodium ions using SP Sephadex-Na cation exchange chromatography. Sephadex G10 and SP Sephadex-Na chromatographies were performed using Flex columns (KIMBLE/KONTES, Vineland, NJ) of dimensions 170 cm × 1.5 cm and 75 cm × 1.5 cm, respectively. For regeneration of the cation exchange column, 1 L of 2 M NaCl solution was used. Water was used as eluent in both chromatographies. Then 5 mL fractions were collected and analyzed by reverse phase-HPLC (RP-HPLC) and/or capillary electrophoresis (CE).

Purity of compounds was assessed using RP-HPLC as well as CE. RP-HPLC analysis was carried out on a Shimadzu chromatography system using Waters Atlantis dC18 column (5 μ, 4.6 mm × 250 mm). The mobile phase consisted of a 100 mM NaCl aqueous solution−CH_3CN mixture (7:3 v/v) run at a constant flow rate of 0.5 mL/min. Compounds were detected at either 254 and/or 215 nm. The purity of each sulfated compound, as determined by RP-HPLC, was greater than 95%. CE experiments were performed using a Beckman P/ACE MDQ system (Fullerton, CA). Electrophoresis was performed at 25 °C and a constant voltage of 8 kV or a constant current of 75 μA using an uncoated fused silica capillary (ID 75 μm) with the total and effective lengths of 31.2 and 21 cm, respectively. A sequential wash of 1 M HCl (10 min), water (3 min), 1 M NaOH (10 min), and water (3 min) at 20 psi was used to activate the capillary. Before each run, the capillary was rinsed with the run buffer; 50 mM sodium phosphate buffer of pH = 3, for 3 min at 20 psi. Sulfated compounds injected at the cathode (0.5 psi for 4 s) and detected at the anode (214 nm).

General Procedure for Horner−Wadsworth−Emmons Reaction. To a solution of (±)-Boc-α-phosphono glycine trimethyl ester (1.2 equiv) in dry THF (3 mL) was added DBU (1.2 equiv), and the mixture was stirred for 30 min at 0 °C. A solution of 3,4-dimethoxy benzaldehyde **9** or 2,5-dimethoxy benzaldehyde **10** (1.0 equivalent) in dry THF (3 mL) was then added slowly, and the reaction mixture was warmed to RT and kept running overnight. After the solvent was removed under reduced pressure, the residue was dissolved in EtOAc (50 mL), quickly washed with saturated aqueous solutions of $NaHCO_3$ (2 × 20 mL), brine (20 mL), and then dried over anhydrous Na_2SO_4. The solvent was evaporated and the crude product purified by flash chromatography on silica gel using (30:70 of EtOAc:hexanes) as mobile phase to yield the desired methyl acrylate in 77−85% yield.

Methyl 2-(*tert*-Butoxycarbonylamino)-3-(3,4-dimethoxyphenyl)acrylate. ^{1}H NMR ($CDCl_3$, 400 MHz): 7.20 (s, 1 H), 7.14 (s, 1 H), 7.07 (d, J = 8.36 Hz, 1 H), 6.80−6.77 (dd, J = 8.36 Hz, J = 1.44 Hz, 1 H), 6.07 (s, br, 1 H), 3.83 (s, 3 H), 3.8 (s, 3 H), 3.77 (s, 3 H), 1.34 (s, 9H). ^{13}C NMR ($CDCl_3$, 100 MHz): 166.22, 153.05, 150.15, 148.7, 131.5, 126.87, 124.09, 122.58, 112.28, 110.86, 80.79, 55.86, 55.73, 52.42, 28.13. MS (ESI) calculated for $C_{17}H_{23}NO_6$, $[M + H]^+$, m/z 338.15, found for $[M + Na]^+$, m/z 360.12.

Methyl 2-(*tert*-Butoxycarbonylamino)-3-(2,5-dimethoxyphenyl)acrylate. ^{1}H NMR ($CDCl_3$, 400 MHz): 7.21 (s, 1 H), 7.0 (s, 1H), 6.78 (t, J = 0.92 H, 2 H), 6.41 (s, br, 1H), 3.77 (s, 3H), 3.76 (s, 3H), 3.68 (s, 3H), 1.32 (s, 9H). ^{13}C NMR ($CDCl_3$, 100 MHz): 166.07, 153.44, 152.81, 151.51, 126.13, 123.79, 123.47, 116.11, 114.52, 112.61, 80.68, 56.45, 55.7, 52.44, 28.27. MS (ESI) calculated for $C_{17}H_{23}NO_6$, $[M + H]^+$, m/z 338.15, found for $[M + Na]^+$, m/z 360.18.

General Procedure for Catalytic Hydrogenation of α-Amino-*β*-aryl Methyl Acrylates. Methyl acrylate from the above reaction and 10% Pd/C were mixed in ethanol (10 mL). Hydrogen gas was then pumped into the mixture at RT. After stirring the solution for 5 h, the catalyst was filtered on Celite and the organic filtrate concentrated in vacuo to afford the reduced product in ∼100% yield.

Methyl 2-(*tert*-Butoxycarbonylamino)-3-(3,4-dimethoxyphenyl)propanoate (11). ^{1}H NMR ($CDCl_3$, 400 MHz): 6.72 (d, J = 8.08 Hz, 1 H), 6.59 (d, J = 8.28 Hz, 1 H), 6.57 (d, J = 1.36 Hz, 1 H), 4.89 (d, J = 7 Hz, 1 H), 4.49−4.43 (dd, J = 13.24 Hz, J = 6.76 Hz, 1 H), 3.79 (s, 3 H), 3.78 (s, 3 H), 3.65 (s, 3 H), 2.96 (t, J = 6.2 Hz, 2 H), 1.35 (s, 9H). ^{13}C NMR ($CDCl_3$, 100 MHz): 172.39, 155.05, 148.91, 148.14, 128.44, 121.38, 112.45, 111.3, 79.89, 55.87, 55.8, 54.50, 52.16, 37.9, 28.3. MS (ESI) calculated for $C_{17}H_{25}NO_6$, $[M + H]^+$, m/z 340.17, found for $[M + Na]^+$, m/z 362.33.

Methyl 2-(*tert*-Butoxycarbonylamino)-3-(2,5-dimethoxyphenyl)propanoate (12). ^{1}H NMR ($CDCl_3$, 400 MHz): 6.7−6.68 (m, 2H), 6.605 (d, J = 2.76 Hz, 1 H), 5.19 (d, J = 7.08 Hz, 1 H), 4.45−4.39 (dd, J = 13.24 Hz, J = 7.04 Hz, 1 H), 3.71 (s, 3H), 3.67 (s, 3H), 3.64 (s, 3H), 2.96 (t, J = 4.84 Hz, 2H), 1.31 (s, 9H). ^{13}C NMR ($CDCl_3$, 100 MHz): 172.7, 155.21, 153.5, 151.82, 125.73, 117.16, 112.7, 111.29, 79.47, 55.77, 55.6, 54.08, 51.97, 32.86, 28.22. MS (ESI) calculated for $C_{17}H_{25}NO_6$, $[M + H]^+$, m/z 340.17, found for $[M + Na]^+$, m/z 361.82.

General Procedure for *N*-Boc Deprotection. To a solution of *N*-Boc *β*-aryl amino ester (1.0 equiv) in CH_2Cl_2 (5 mL), trifluoro-acetic acid (TFA, 5 mL) was added dropwise at 0 °C and the mixture was warmed to RT. After stirring for 4 h, the reaction mixture was diluted with CH_2Cl_2 (25 mL) and neutralized by dropwise addition of saturated aqueous $NaHCO_3$ (20 mL). The organic layer was separated, and the aqueous phase was extracted with EtOAc (2 × 25 mL). The organic extracts were combined, washed with saturated NaCl solution (25 mL), and dried over anhydrous Na_2SO_4. Removal of the solvent under reduced pressure left a residue, which was purified by silica gel chromatography (90:10 of EtOAc:hexanes) to afford the desired *β*-aryl amino ester in ∼85% yield.

Methyl 3,4-Dimethoxy Phenylalanine. ^{1}H NMR ($CDCl_3$, 400 MHz): 6.73 (d, J = 7.76 Hz,1 H), 6.66 (d, J = 7.36 Hz, 1 H), 6.65 (s, 1 H), 3.79−3.65 (m, 1 H), 3.79 (s, 3 H), 3.78 (s, 3H), 3.64 (s, 3H), 2.99−2.95 (dd, J = 13.6 Hz, J = 4.84 Hz, 1H), 2.79−2.74 (dd, J = 13.6 Hz, J = 7.64 Hz, 1H), 1.86 (s, 1 H). ^{13}C NMR ($CDCl_3$, 100 MHz): 175.22, 148.96, 147.99, 129.49,121.36, 112.4, 111.32, 55.87, 55.83, 55.8, 51.99, 40.41. MS (ESI) calculated for $C_{12}H_{17}NO_4$, $[M + H]^+$, m/z 240.12, found for $[M + Na]^+$, m/z 262.22.

Methyl 2,5-Dimethoxy Phenylalanine. ^{1}H NMR ($CDCl_3$, 400 MHz): 6.71 (s, 3H), 4.28−4.25 (dd, J = 8 Hz, J = 5 Hz, 1H), 3.70 (s, 3H), 3.66 (s, 3H), 3.63 (s, 3H), 3.33−3.28 (dd, J = 14.12 Hz, J = 4.95 Hz, 1 H), 3.03−2.97 (dd, J = 14.12 Hz, J = 8.04 Hz, 1H). ^{13}C NMR ($CDCl_3$, 100 MHz): 169.51, 153.41, 151.81, 123.01, 117.87, 113.92, 111.67, 55.77, 53.04, 52.77, 32.01. MS (ESI) calculated for $C_{12}H_{17}NO_4$, $[M + H]^+$, m/z 240.12, found for $[M + Na]^+$, m/z 262.15.

General Procedure for Pictet−Spengler Reaction of Substituted Methyl Phenylalanine Esters and Substituted Phenethylamine. A solution of methyl phenylalanine derivative or phenethylamine derivative (1 equiv) in CH_2Cl_2 (2 mL) was treated at RT with formaldehyde (37% aqueous solution, 1.5 equiv). TFA (2 equivalent) was then slowly added over 15 min. After stirring for 5 h, the reaction mixture was diluted with CH_2Cl_2 (2 mL) and neutralized with saturated $NaHCO_3$ solution (5 mL). The organic layer was separated, and the aqueous phase was further extracted with CH_2Cl_2 (3 × 10 mL). The organic extracts were combined, washed with saturated NaCl solution (10 mL), and dried over anhydrous Na_2SO_4. Removal of the solvent under reduced pressure left a residue, which was purified by silica gel chromatography (60:40 of EtOAc:hexanes) to yield the desired tetrahydroisoquinoline derivative in 70−80% yield.

Methyl 6,7-Dimethoxy-1,2,3,4-tetrahydroisoquinoline-3-carboxylate (13). ^{1}H NMR ($CDCl_3$, 400 MHz): 6.52 (s, 1 H), 6.46 (s, 1 H), 4.08−3.98 (dd, J = 25.64 Hz, J = 15.67 Hz, 2 H), 3.79−3.73 (m, 1 H), 3.78 (s, 3 H), 3.77 (s, 3 H), 3.72 (s, 3 H), 3.41 (s, br, 1 H), 3.00−2.95 (dd, J = 16.08 Hz, J = 4.76 Hz, 1 H), 2.91−2.84 (dd, J = 16 Hz, J = 9.68 Hz, 1 H). ^{13}C NMR ($CDCl_3$, 100 MHz): 172.73, 147.83, 125.48, 124.35, 111.72, 108.91, 55.93, 55.57, 52.34, 46.37, 30.63. MS (ESI) calculated for $C_{13}H_{17}NO_4$, $[M + H]^+$, m/z 252.12, found for $[M + Na]^+$, m/z 274.19.

Methyl 5,8-Dimethoxy-1,2,3,4-tetrahydroisoquinoline-3-carboxylate (14). ^{1}H NMR ($CDCl_3$, 400 MHz): 6.53−6.52 (m, 2H), 3.94−3.81 (m, 3H), 3.69 (s, 3H), 3.67 (s, 3H), 3.48 (s, 3H), 3.15−3.06 (m, 1H), 2.87−2.79 (m, 1H). ^{13}C NMR ($CDCl_3$, 100 MHz): 173.45, 151.16, 150.15, 124.81, 123.19, 107.12, 56.70, 55.67, 51.21, 45.55, 25.87. MS (ESI) calculated for $C_{13}H_{17}NO_4$, $[M + H]^+$, m/z 252.12, found m/z 252.14.

5,6-Dimethoxy-1,2,3,4-tetrahydroisquinoline (2). ^{1}H NMR ($CDCl_3$, 400 MHz): 6.67−6.66 (m, 2 H), 3.75 (s, 3H), 3.73 (s, 3H), 3.59 (s, 1 H), 3.16 (s, 1 H), 2.8 (t, J = 5.16 Hz, 2 H), 2.74 (t, J = 5.08 Hz, 2 H). ^{13}C NMR ($CDCl_3$, 100 MHz): 150.64, 146.63, 129.23, 128.41, 121.92, 110.41, 59.97, 55.92, 53.99, 48.88, 23.90. MS (ESI) calculated for $C_{11}H_{15}NO_2$, $[M + H]^+$, m/z 194.11, found for $[M + Na]^+$, m/z 216.11.

General Procedure for *N*-Arylacylation of 1,2,3,4-Tetrahydroisoquinoline-3-carboxylic Acid Methyl Ester (THIQ3CA Ester) and 1,2,3,4-Tetrahydroisoquinoline (THIQ). To a stirred solution of either 2,5-dimethoxylphenyl acetic, propionic, or butanoic acid (1 equiv) in anhydrous CH_2Cl_2 (5 mL) was added 1-ethyl-3-(3-dimethylaminopropyl)carbodiimide (EDCI, 1.1 equiv) and DMAP (1.1 equival) at RT under nitrogen atmosphere. Dimethoxy-1,2,3,4-tetrahydroisoquinoline (either **1**, **2**, **13**, or **14**) (1.1 equiv) in anhydrous CH_2Cl_2 (5 mL) was then added dropwise. After stirring overnight, the reaction mixture was partitioned between 2 N HCl solution (20 mL) and CH_2Cl_2 (30 mL). The organic layer was washed further with 2 N HCl (2 × 10 mL) and saturated NaCl solution (20 mL), dried using anhydrous Na_2SO_4, and concentrated to give a crude, which purified by silica gel chromatography (50:50 of EtOAc:hexanes) to give the desired coupled product in 70−95% yield.

Methyl 2-(2-(2,5-Dimethoxyphenyl)acetyl)-6,7-dimethoxy-1,2,3,4-tetrahydroisoquinoline-3-carboxylate (15a). ^{1}H NMR ($CDCl_3$, 400 MHz): 6.80 (d, J = 2.64 Hz, 1 H), 6.75−6.67 (m, 2 H), 6.56−6.40 (m, 2 H), 5.51−5.49 and 4.94−4.92 (dd and dd, J = 3.32 Hz, J = 6.04 Hz and J = 2.32 Hz, J = 5.76 Hz, 1 H) 4.91−4.30 (m, 2 H), 3.78 (s, 2 H), 3.76 (s, 3 H), 3.75 (s, 3 H), 3.72 (s, 3 H), 3.66 (s, 3H), 3.50 (d, J = 51.52 Hz, 3 H), 3.14−3.06 (m, 1 H), 3.02−2.84 (m, 1 H). ^{13}C NMR ($CDCl_3$, 100 MHz): 171.49, 171.36, 153.78, 151.18, 150.55, 148.22, 124.28, 123.92, 122.83, 115.91, 113.31, 112.90, 111.58, 109.28, 56.1, 55.95, 55.91, 55.73, 52.44, 52.29, 45.47, 35.30, 31.23. MS (ESI) calculated for $C_{23}H_{27}NO_7$, $[M + H]^+$, m/z 430.18, found for $[M + Na]^+$, m/z 452.36.

Methyl 2-(2-(2,5-Dimethoxyphenyl)acetyl)-5,8-dimethoxy-1,2,3,4-tetrahydroisoquinoline-3-carboxylate (16a). ^{1}H NMR ($CDCl_3$, 400 MHz): 6.82−6.79 (m, 1 H), 6.73−6.66 (m, 2 H), 6.60−6.54 (m, 2 H), 5.64−5.62 and 4.96−4.94 (dd and dd, J = 2.36 Hz, J = 6.80 Hz and J = 1.56 Hz, J = 6.44 Hz, 1 H), 5.02−4.14 (m, 2 H), 3.76 (d, J = 23.76 Hz, 2H), 3.71 (s, 3H), 3.70 (s, 3 H), 3.67 (s, 3 H), 3.65 (s, 3 H), 3.49 (d, J = 46.72 Hz, 3 H), 3.41−3.37 (m, 1 H), 2.78−2.49 (m, 1 H). ^{13}C NMR ($CDCl_3$, 100 MHz): 171.74, 171.45, 153.64, 151.30, 150.93, 149.57, 124.35, 122.29, 121.94, 116.04, 113.00, 111.39, 108.13, 107.43, 56.02, 55.83, 55.70, 55.42, 52.24, 49.92, 41.23, 35.06, 24.27. MS (ESI) calculated for $C_{23}H_{27}NO_7$, $[M + H]^+$, m/z 430.18, found for $[M + Na]^+$, m/z 452.3.

Methyl 2-(3-(2,5-Dimethoxyphenyl)propanoyl)-6,7-dimethoxy-1,2,3,4-tetrahydroisoquinoline-3-carboxylate (15b). ^{1}H NMR ($CDCl_3$, 400 MHz): 6.72−6.69 (m, 3 H), 6.64−6.45 (m, 2 H), 5.52−5.50 and 4.87−4.85 (dd and dd, J = 3 Hz, J = 6.08 Hz and J = 2.44 Hz, J = 5.76 Hz, 1 H), 4.88−4.30 (m, 2 H), 3.78 (s, 3 H), 3.75 (s, 3 H), 3.73 (s, 3 H), 3.67 (s, 3 H), 3.56 (s, 3 H), 3.78−3.09 (m, 1 H), 2.99−2.84 (m, 3 H), 2.70−2.67 (m, 2 H). ^{13}C NMR ($CDCl_3$,100 MHz): 172.77, 171.62, 153.58, 151.76, 148.26, 147.80, 130.65, 124.10, 123.70, 116.74, 111.71, 111.26, 109.36, 108.91, 55.94, 55.91, 55.80, 55.67, 52.77, 50.97, 45.12, 34.18, 30.26, 26.69. MS (ESI) calculated for $C_{24}H_{29}NO_7$, $[M + H]^+$, m/z 444.19, found for $[M + Na]^+$, m/z 466.04.

Methyl 2-(3-(2,5-Dimethoxyphenyl)propanoyl)-5,8-dimethoxy-1,2,3,4-tetrahydroisoquinoline-3-carboxylate (16b). ^{1}H NMR ($CDCl_3$, 400 MHz): 6.73−6.54 (m, 5 H), 5.65−5.63 and 4.96−4.94 (dd and dd, J = 2.20 Hz, J = 6.76 Hz and J = 1.60 Hz, J = 6.40 Hz, 1 H), 5.03−4.14 (m, 2 H), 3.73 (s, 3 H), 3.70 (s, 3 H), 3.69 (s, 3 H), 3.67 (s, 3 H), 3.55 (s, 3 H), 3.54−3.38 (m, 1 H), 2.94−2.85 (m, 2 H), 2.78−2.53 (m, 3 H). ^{13}C NMR ($CDCl_3$, 100 MHz): 173.16, 171.58, 153.60, 151.81, 150.92, 149.59, 130.67, 122.43, 121.71, 116.50, 111.81, 111.20, 108.09, 107.63, 55.83, 55.70, 55.44, 55.31, 52.31, 49.61, 40.96, 34.16, 26.71, 24.31. MS (ESI) calculated for $C_{24}H_{29}NO_7$, $[M + H]^+$, m/z 444.19, found for $[M + Na]^+$, m/z 465.97.

Methyl 2-(4-(2,5-Dimethoxyphenyl)butanoyl)-6,7-dimethoxy-1,2,3,4-tetrahydroisoquinoline-3-carboxylate (15c). ^{1}H NMR ($CDCl_3$, 400 MHz): 6.71−6.62 (m, 3 H), 6.55−6.47 (m, 2 H), 5.52−5.50 and 4.69−4.67 (dd and dd, J = 2.88 Hz, J = 5.92 Hz and J = 2.36 Hz, J = 5.56 Hz, 1 H), 4.86−4.44 (m, 2 H), 3.78 (s, 3 H), 3.77 (s, 3 H), 3.69 (s, 3 H), 3.68 (s, 3 H), 3.55 (s, 3 H), 3.17−3.09 (m, 1 H), 3.04−2.93 (m, 1 H), 2.58−2.64 (m, 2 H), 2.44−2.40 (m, 2 H), 1.97−1.89 (m, 2 H). ^{13}C NMR ($CDCl_3$, 100 MHz): 173.18, 171.55, 153.50, 151.88, 148.28, 147.84, 131.32, 124.11, 123.60, 116.45, 111.30, 110.97, 109.38, 108.99, 55.96, 55.94, 55.90, 55.70, 52.30, 50.94, 45.16, 33.10, 30.27, 29.76, 24.81. MS (ESI) calculated for $C_{25}H_{31}NO_7$, $[M + H]^+$, m/z 458.21, found for $[M + Na]^+$, m/z 479.96.

Methyl 2-(4-(2,5-Dimethoxyphenyl)butanoyl)-5,8-dimethoxy-1,2,3,4-tetrahydroisoquinoline-3-carboxylate (16c). ^{1}H NMR ($CDCl_3$, 400 MHz): 6.70−6.55 (m, 5 H), 5.63−5.60 and 4.72 (dd and d, J = 2.32 Hz, J = 6.76 Hz and J = 4.92 Hz, 1 H), 5.02−4.09 (m, 2 H), 3.71 (s, 3 H), 3.70 (s, 3 H), 3.69 (s, 3 H), 3.67 (s, 3 H), 3.55 (s, 3 H), 3.40−3.37 (m, 1 H), 2.75−2.68 (m, 1 H), 2.66−2.53 (m, 2 H), 2.51−2.31 (m, 2 H), 1.97−1.89 (m, 2 H). ^{13}C NMR ($CDCl_3$, 100 MHz): 173.44, 171.62, 153.50, 151.85, 150.93, 149.58, 131.47, 122.5, 121.75, 116.38, 111.48, 111.18, 108.17, 107.38, 55.83, 55.75, 55.69, 55.40, 52.29, 49.64, 40.89, 33.26, 29.93, 25.12, 24.30. MS (ESI) calculated for $C_{25}H_{31}NO_7$, $[M + H]^+$, m/z 458.21, found for $[M + Na]^+$, m/z 480.4.

1-(6,7-Dimethoxy-3,4-dihydroisoquinolin-2(1*H*)-yl)-2-(2,5-dimethoxy phenyl) Ethanone (3). ^{1}H NMR ($CDCl_3$, 400 MHz): 6.78−6.64 (m, 5H), 4.54 (d, J = 48.84 Hz, 2H), 3.76 (s, 3H), 3.71(s, 3H), 3.69 (s, 3H), 3.67(s, 3H), 3.63−3.60 (m, 3H), 3.58−3.54 (m, 1H), 2.78 (t, J = 5.96 Hz, 1 H), 2.64 (t, J = 5.88 Hz, 1 H). ^{13}C NMR ($CDCl_3$, 100 MHz): 170.40, 153.68, 151.00, 146.18, 128.52, 126.68, 124.67, 121.98, 117.10, 115.81, 112.94, 111.57, 110.88, 60.28, 56.09, 55.87, 55.68, 47.17, 43.89, 35.09, 23.64. MS (ESI) calculated for $C_{21}H_{25}NO_5$, $[M + H]^+$, m/z 372.17, found for $[M + Na]^+$, m/z 394.33.

1-(5,6-Dimethoxy-3,4-dihydroisoquinolin-2(1*H*)-yl)-4-(2,5-dimethoxy phenyl) Butan-1-one (4). ^{1}H NMR ($CDCl_3$, 400 MHz): 6.79−6.60 (m, 5 H), 4.49 (d, J = 74.72 Hz, 2 H), 3.77 (s, 3H), 3.73 (s, 3H), 3.67 (s, 3H), 3.66 (s, 3H), 3.67−3.66 (m, 1 H), 3.50 (t, J = 5.68 Hz, 1 H), 2.80−2.76 (m, 2 H), 2.59 (t, J = 7.6 Hz, 2 H), 2.34 (t, J = 7.36 Hz, 2 H), 1.92−1.88 (m, 2H). ^{13}C NMR ($CDCl_3$, 100 MHz): 171.92, 153.48, 151.83, 150.88, 146.21, 131.34, 128.44, 126.86, 126.00, 121.97, 121.27, 116.33, 111.22, 60.34, 55.90, 55.87, 55.68, 46.83, 42.92, 39.34, 33.05, 29.92, 25.19. MS (ESI) calculated for $C_{23}H_{29}NO_5$, $[M + H]^+$, m/z 400.20, found for $[M + Na]^+$, m/z 422.37.

General Procedure for *O*-Demethylation of *N*-Arylacyl-THIQ3CA Esters and THIQs. To a stirred solution of the protected THIQ3CA ester (or THIQ derivative) in anhydrous CH_2Cl_2 (5 mL), BBr_3 (1 M solution in CH_2Cl_2, 9−12 equiv) was added dropwise at −78 °C under nitrogen atmosphere over 10 min. After 2 h, the reaction mixture was brought to RT and allowed to equilibrate overnight. A mixture of (1:1) methanol/water (2 mL) was then added slowly at 0 °C and vigorously stirred for 10 min to quench the reaction. The reaction mixture was then concentrated and partitioned between EtOAc (25 mL)

dx.doi.org/10.1021/jm2008387 |*J. Med. Chem.* 2011, 54, 6125–6138

and saturated solution of NH_4Cl (15 mL). The aqueous layer was further washed with EtOAc (2 × 20 mL). The combined organic layer was washed with brine solution (15 mL), dried using anhydrous Na_2SO_4, and finally concentrated in vacuo. The crude was purified by gradient silica gel chromatography using EtOAc in hexanes to give the desired poly phenol of THIQ derivatives in 65−85% yield.

2-(2-(2,5-Dihydroxyphenyl)acetyl)-6,7-dihydroxy-1,2,3,4-tetrahydroisoquinoline-3-carboxylic Acid (17a). ^{1}H NMR (acetone-d_6, 400 MHz): 6.65 (d, J = 2.92 Hz, 1 H), 6.54−6.50 (m, 3 H), 6.47−6.44 (dd, J = 2.96 Hz, J = 8.56 Hz, 1 H), 5.20−5.18 and 5.15−5.13 (dd and dd, J = 3.60 Hz, J = 5.92 Hz and J = 2.60 Hz, J = 5.68 Hz, 1 H), 4.79−4.19 (m, 2 H), 3.78−3.43 (m, 2 H), 3.07−3.00 (m, 1 H), 2.88−2.84 (m, 1 H). ^{13}C NMR (acetone-d_6, 100 MHz): 173.3, 172.2, 151.33, 149.87, 149.53, 145.04, 124.65, 124.52, 123.98, 118.48, 117.87, 115.69, 115.53, 113.83, 56.18, 46.50, 36.49, 31.68. MS (ESI) calculated for $C_{18}H_{17}NO_7$, $[M + H]^+$, m/z 360.1, found for $[M + Na]^+$, m/z 382.24.

2-(2-(2,5-Dihydroxyphenyl)acetyl)-5,8-dihydroxy-1,2,3,4-tetrahydroisoquinoline-3-carboxylic Acid (18a). ^{1}H NMR (acetone-d_6, 400 MHz): 6.64−6.54 (m, 3 H), 6.47−6.42 (m, 2 H), 5.49−5.47 and 5.26 (dd and d, J = 2.20 Hz, J = 6.32 Hz and J = 5.00 Hz, 1 H), 4.91−4.19 (m, 2 H), 3.86−3.81 (dd, J = 5.84 Hz, J = 14.68 Hz, 1 H), 3.72−3.57 (m, 1 H), 3.46−3.41 (m, 1 H), 2.71−2.55 (m, 1 H).^{13}C NMR (acetone-d_6, 100 MHz): 173.73, 172.51, 151.32, 149.58, 148.19, 147.02, 123.21, 121.08, 120.82, 118.53, 117.59, 116.68, 115.50, 113.46, 51.13, 42.68, 36.41, 25.43. MS (ESI) calculated for $C_{18}H_{17}NO_7$, $[M + H]^+$, m/z 360.1, found for $[M + Na]^+$, m/z 382.21.

2-(3-(2,5-Dihydroxyphenyl)propanoyl)-6,7-dihydroxy-1,2,3,4-tetrahydroisoquinoline-3-carboxylic Acid (17b). ^{1}H NMR (400 MHz, acetone-d_6): 6.55−6.47 (m, 4 H), 6.40−6.38 (dd, J = 2.88 Hz, J = 8.56 Hz, 1 H), 5.22−5.20 and 4.94−4.93 (dd and dd, J = 3.66 Hz, J = 6.00 Hz and J = 2.68 Hz, J = 5.68 Hz, 1 H), 4.58−4.17 (m, 2 H), 3.07−2.94 (m, 1 H), 2.91−2.80 (m, 1 H), 2.79−2.66 (m, 4 H). ^{13}C NMR (100 MHz, acetone-d_6): 174.36, 172.4, 151.36, 149.13, 145.02, 144.81, 129.95, 124.77, 124.58, 117.85, 117.66, 115.69, 114.7, 113.86, 55.41, 45.78, 35.63, 30.93. 26.11. MS (ESI) calculated for $C_{19}H_{19}NO_7$, $[M + H]^+$, m/z 374.12, found for $[M + Na]^+$, m/z 396.22.

2-(3-(2,5-Dihydroxyphenyl)propanoyl)-5,8-dihydroxy-1,2,3,4-tetrahydroisoquinoline-3-carboxylic Acid (18b). ^{1}H NMR (CD_3OD, 400 MHz): 6.53−6.47 (m, 2H), 6.43−6.35 (m, 3 H), 5.34−5.32 and 5.01−5.00 (dd and dd, J = 2.80 Hz, J = 6.48 Hz and J = 2.04 Hz, J = 6.12 Hz, 1 H), 4.82−4.19 (m, 2 H), 3.46−3.31 (m, 1 H), 2.81−2.63 (m, 4 H), 2.56−2.46 (m, 1 H). ^{13}C NMR (CD_3OD, 100 MHz): 175.91, 174.51, 151.24, 149.26, 148.40, 147.41, 129.59, 124.20, 121.19, 117.75, 117.17, 114.81, 114.25, 113.79, 52.05, 42.43, 35.20, 30.68, 27.25. MS (ESI) calculated for $C_{19}H_{19}NO_7$, $[M + H]^+$, m/z 374.12, found for $[M + Na]^+$, m/z 396.2.

2-(4-(2,5-Dihydroxyphenyl)butanoyl)-6,7-dihydroxy-1,2,3,4-tetrahydroisoquinoline-3-carboxylic Acid (17c). ^{1}H NMR (acetone-d_6, 400 MHz): 6.55−6.46 (m, 4 H), 6.40−6.38 (m,1 H), 5.25−5.23 and 4.91−4.88 (dd and dd, J = 3.44 Hz, J = 6.00 Hz and J = 2.60 Hz, J = 5.52 Hz, 1 H), 4.64−4.17 (m, 2 H), 3.09−3.00 (m, 1 H), 2.98−2.83 (m, 1H), 2.49−2.17 (m, 4 H), 1.83−1.81 (m, 2 H). ^{13}C NMR (acetone-d_6, 100 MHz): 174.09, 172.63, 151.06, 149.23, 145.05, 144.98, 129.65, 124.81, 124.7, 124.1, 117.45, 116.89, 115.73, 114.27, 113.88, 55.39, 45.72, 36.27, 33.12, 31.73, 26.14. MS (ESI) calculated for $C_{20}H_{21}NO_7$, $[M + H]^+$, m/z 388.13, found for $[M + Na]^+$, m/z 410.21.

2-(4-(2,5-Dihydroxyphenyl)butanoyl)-5,8-dihydroxy-1,2,3,4-tetrahydroisoquinoline-3-carboxylic Acid (18c). ^{1}H NMR (acetone-d_6, 400 MHz): 6.53−6.43 (m, 4 H), 6.40−6.36 (m, 1 H), 5.50−5.48 and 5.03−5.01 (dd and dd, J = 2.52 Hz, J = 6.68 and J = 1.88 Hz, J = 6.32 Hz, 1 H), 4.90−4.14 (m, 2 H), 3.53−3.40 (m, 1 H), 2.81−2.66 (m, 1 H), 2.54−2.33 (m, 4 H), 1.83−1.75 (m, 2 H). ^{13}C NMR (acetone-d_6, 100 MHz): 174.17, 172.60, 150.99, 149.15, 148.28, 146.99, 129.62, 121.51, 117.30, 116.80, 114.17, 113.64, 113.33, 113.18, 54.44, 50.65, 41.81, 33.14, 26.24, 25.38. MS (ESI) calculated for $C_{20}H_{21}NO_7$, $[M + H]^+$, m/z 388.13, found for $[M + Na]^+$, m/z 410.34.

1-(6,7-Dihydroxy-3,4-dihydroisoquinolin-2(1*H*)-yl)-2-(2,5-dihydroxyphenyl) Ethanone (5). ^{1}H NMR (acetone-d_6, 400 MHz): 6.60−6.53 (m, 2 H), 6.48−6.44 (m, 3 H), 4.5 (d, J = 84.0 Hz, 2 H), 3.72 (t, J = 5.72 Hz, 1 H), 3.63 (d, J = 6.96 Hz, 2 H), 3.58 (t, J = 5.96 Hz, 1 H), 2.56 (t, J = 5.60 Hz, 1 H), 2.51 (t, J = 5.88 Hz, 1 H). ^{13}C NMR (acetone-d_6, 100 MHz): 172.25, 151.30, 150.12, 144.84, 144.65, 126.76, 125.22, 124.87, 123.44, 118.06, 115.84, 115.58, 113.79, 48.14, 45.17, 36.63, 28.33. MS (ESI) calculated for $C_{17}H_{17}NO_5$, $[M + H]^+$, m/z 316.11, found for $[M + Na]^+$, m/z 338.2.

1-(5,6-Dihydroxy-3,4-dihydroisoquinolin-2(1*H*)-yl)-4-(2,5-dihydroxyyphenyl) Butan-1-one (6). ^{1}H NMR (CD_3OD, 400 MHz): 6.55−6.49 (m, 2 H), 6.46−6.43 (m, 1 H), 6.39−6.32 (m, 2 H), 4.39 (d, J = 43.04 Hz, 2 H), 3.6 (t, J = 6.16 Hz, 1 H), 3.49 (t, J = 6.04 Hz, 1 H), 2.68 (t, J = 5.92 Hz, 1 H), 2.63 (t, J = 6.12 Hz, 1 H), 2.50−2.45 (m, 2 H), 2.35−2.30 (m, 2 H), 1.81−1.74 (m, 2 H). ^{13}C NMR (CD_3OD, 100 MHz): 174.58, 151.10, 149.33, 144.64, 143.76, 130.19, 126.20, 125.94, 123.48, 118.24, 117.83, 116.93, 114.50, 45.03, 44.48, 41.11, 33.96, 30.85, 26.77. MS (ESI) calculated for $C_{19}H_{21}NO_5$, $[M + H]^+$, m/z 344.14, found for $[M + Na]^+$, m/z 366.23.

General Procedure for *O*-Sulfonation of Polyphenolic THIQ3CA and THIQ Derivatives. An equivolume mixture of anhydrous CH_3CN and DMF (3 mL) containing THIQ polyphenol and SO_3:NMe_3 complex (6 equiv/−OH group of the polyphenol) was heated for 5 h at 80 °C. Following reaction, the solution was cooled and concentrated in vacuo at less than 35 °C and the residue taken up in water for loading onto a Sephadex G10 column. The column was eluted with deionized water, and fractions were combined based on RP-HPLC and/or CE profiles (see above). The eluted fractions were lyophilized and reloaded onto a SP Sephadex column for sodium exchange. Appropriate fractions were pooled, concentrated in vacuo, and lyophilized to obtain a white powder of per-sulfated THIQ-based antithrombin activators in 45−75% yield.

Sodium 2-(2-(2,5-Di-*O*-sulfonato-phenyl)acetyl)-6,7-di-*O*-sulfonato-1,2,3,4-tetrahydroisoquinoline-3-carboxylate Tetrasodium (19a). ^{1}H NMR (D_2O, 400 MHz): 7.47−7.25 (m, 5 H), 5.02−4.99 and 4.93−4.91 (dd and dd, J = 3.68 Hz, J = 5.56 Hz and J = 2.64 Hz, J = 5.32 Hz, 1 H), 4.90−4.82 (m, 2 H), 4.27−3.56 (m, 2 H), 3.32−3.12 (m, 2 H). ^{13}C NMR (D_2O, 100 MHz): 177.74, 172.94, 148.70, 147.52, 141.95, 132.61, 132.16, 131.31, 129.91, 124.43, 122.91, 122.35, 121.65, 121.05, 55.59, 45.86, 35.39, 31.88. MS (ESI) calculated for $C_{18}H1_2NNa_5O_{19}S_4$, $[M\text{-}H]^-$, m/z 787.84, found for $[M - Na]^-$, m/z 765.92.

Sodium 2-(2-(2,5-Di-*O*-sulfonato-phenyl)acetyl)-5,8-di-*O*-sulfonato-1,2,3,4-tetrahydroisoquinoline-3-carboxylate Tetrasodium (20a). ^{1}H NMR (D_2O, 400 MHz): 7.09−7.32 (m, 5 H), 4.87−5.18 (m, 1 H), 4.66−4.84 (m, 2 H), 3.52−4.14 (m, 2 H), 3.28−3.44 (m, 1 H), 2.88−2.99 (m, 1 H). ^{13}C NMR (D_2O, 100 MHz): 176.65, 172.60, 148.65, 147.67, 146.05, 144.95, 129.91, 129.08, 127.82, 124.56, 122.89, 121.59, 120.99, 120.38, 54.08, 41.38, 35.37, 25.88. MS (ESI) calculated for $C_{18}H1_2NNa_5O_{19}S_4$, $[M - H]^-$, m/z 787.84, found for $[M - Na]^-$, m/z 766.05.

Sodium 2-(3-(2,5-Di-*O*-sulfonato-phenyl)propanoyl)-6,7-di-*O*-sulfonato-1,2,3,4-tetrahydroisoquinoline-3-carboxylate Tetrasodium (19b). ^{1}H NMR (D_2O, 400 MHz): 7.27−7.01 (m, 5 H), 5.16−5.13 and 4.98−4.95 (dd and dd, J = 3.76 Hz, J = 5.8 Hz and J = 3.32 Hz, J 5.92 Hz, 1 H), 4.61−4.49 (m, 2 H), 3.18−2.82 (m, 5 H), 2.74−2.52 (m, 1 H). ^{13}C NMR (D_2O, 100 MHz): 175.25, 174.50,

148.72, 147.26, 141.83, 141.57, 134.95, 132.34, 131.36, 130.93, 123.43, 122.65, 122.29, 120.97, 57.54, 45.51, 33.49, 30.79. 26.18. MS (ESI) calculated for $C_{19}H_{14}NNa_5O_{19}S_4$, $[M - H]^-$, m/z 801.85, found for $[M - Na]^-$, m/z 779.97.

Sodium 2-(3-(2,5-Di-*O*-sulfonato-phenyl) propanoyl)-5,8-di-*O*-sulfonato-1,2,3,4-tetrahydroisoquinoline-3-carboxylate Tetrasodium (20b). ^{1}H NMR (D_2O, 400 MHz): 7.45−7.03 (m, 5 H), 5.24−5.03 (m, 1 H), 4.91−4.51 (m, 2 H), 3.52−3.36 (m, 1 H), 3.15−3.08 (m, 3 H), 3.06−2.64 (m, 2 H). ^{13}C NMR (D_2O, 100 MHz): 175.49, 174.57, 148.73, 147.33, 146.23, 145.17, 135.04, 128.84, 127.92, 127.56, 123.43, 122.79, 121.30, 120.53, 56.73, 52.42, 41.27, 33.33, 25.90. MS (ESI) calculated for $C_{19}H_{14}NNa_5O_{19}S_4$, $[M - H]^-$, m/z 801.85, found for $[M - Na]^-$, m/z. 780.07.

Sodium 2-(4-(2,5-Di-*O*-sulfonato-phenyl)butanoyl)-6,7-di-*O*-sulfonato-1,2,3,4-tetrahydroisoquinoline-3-carboxylate Tetrasodium (19c). ^{1}H NMR (D_2O, 400 MHz): 7.24−7.02 (m, 5 H), 5.02−4.99 and 4.94−4.91 (t and dd, J = 5.64 Hz and J = 4.24 Hz, J = 5.92 Hz, 1 H), 4.49−4.35 (m, 2 H), 3.13−2.82 (m, 2 H), 2.66−2.63 (m, 2H), 2.49−2.06 (m, 2 H), 1.93−1.65 (m, 2 H). ^{13}C NMR (D_2O, 100 MHz): 175.71, 172.92, 148.73, 147.35, 142.24, 141.55, 136.16, 132.29, 132.16, 123.51, 122.58, 122.04, 120.72, 120.33, 53.13, 45.87, 37.18, 32.33, 29.49, 25.01. MS (ESI) calculated for $C_{20}H_{16}NNa_5O_{19}S_4$, $[M - H]^-$, m/z 815.87, found for $[M - Na]^-$, m/z 793.7.

Sodium 2-(4-(2,5-Di-*O*-sulfonato-phenyl)butanoyl)-5,8-di-*O*-sulfonato-1,2,3,4-tetrahydroisoquinoline-3-carboxylate Tetrasodium (20c). ^{1}H NMR (D_2O, 400 MHz): 7.42−7.30 (m, 3 H), 7.27−7.16 (m, 2 H), 5.17−4.91 (m, 1 H), 4.88−4.53 (m, 2 H), 3.56−3.33 (m, 1 H), 3.14−2.83 (m, 1 H), 2.8−2.37 (m, 4 H), 2.0−1.9 (m, 2 H). ^{13}C NMR (D_2O, 100 MHz): 177.65, 175.86, 148.76, 147.27, 146.08, 144.89, 136.56, 129.31, 128.66, 127.93, 123.43, 122.54, 121.12, 120.25, 56.58, 41.2, 32.95, 29.1, 26.77, 25.86. MS (ESI) calculated for $C_{20}H_{16}NNa_5O_{19}S_4$, $[M - H]^-$, m/z 815.87, found for $[M - Na]^-$, m/z 793.92.

1-(6,7-Di-*O*-sulfonato-3,4-dihydroisoquinolin-2(1*H*)-yl)-2-(2,5-di-*O*-sulfonato-phenyl) Ethanone Tetrasodium (7). ^{1}H NMR (D_2O, 400 MHz): 7.32−7.29 (m, 2 H), 7.18−7.06 (m, 3 H), 4.59 (d, J = 48.8 Hz, 2 H), 3.84 (s, 2 H), 3.68 (t, J = 5.84 Hz, 1 H), 3.63 (t, J = 6.00 Hz, 1 H), 2.79−2.73 (m, 2 H). ^{13}C NMR (D_2O, 100 MHz): 171.96, 148.73, 147.37, 141.51, 141.37, 133.57, 131.29, 130.01, 124.11, 122.94, 122.68, 121.6, 120.94, 47.08, 44.23, 35.0, 28.21. MS (ESI) calculated for $C_{17}H_{13}NNa_4O_{17}S_4$, $[M - H]^-$, m/z 721.87, found for $[M - Na]^-$, m/z 700.08.

1-(5,6-Di-*O*-sulfonato-3,4-dihydroisoquinolin-2(1*H*)-yl)-4-(2,5-di-*O*-sulfonato-phenyl)butan-1-one Tetrasodium (8). ^{1}H NMR (D_2O, 400 MHz): 7.42−7.16 (m, 5 H), 5.05 (d, J = 8.32 Hz, 2 H), 3.69−3.66 (m, 2 H), 3.07−3.03 (m, 2 H), 2.8−2.74 (m, 2 H), 2.58 (t, J = 7.2 Hz, 1 H), 2.51 (t, J = 7.28, 1 H), 1.96−1.92 (m, 2 H). ^{13}C NMR (D_2O, 100 MHz): 174.9, 148.73, 147.32, 143.05, 142.49, 137.64, 136.36, 134.21, 133.61, 130.12, 123.5, 122.52, 120.35, 42.49, 41.88, 39.87, 32.73, 29.01, 26.80. MS (ESI) calculated for $C_{19}H_{17}NNa_4O_{17}S_4$, $[M - H]^-$, m/z 749.9, found for $[M - Na]^-$, m/z 727.96.

Equilibrium Binding Studies. Fluorescence spectroscopy experiments were performed using a QM4 fluorometer (Photon Technology International, Birmingham, NJ) in 20 mM sodium phosphate buffer, pH 6.0, containing 25 mM NaCl, 0.1 mM EDTA, and 0.1% PEG8000 at 25 °C in a manner following our previous work.[5,31] Equilibrium dissociation constants (K_D) for the interaction of nonsaccharide aromatic activators with plasma AT were determined by titrating the activator (ACT) into a solution of serpin and monitoring the decrease in the fluorescence at 340 nm (λ_{EX} = 280 nm). Slit widths were 1 mm on both the excitation and emission sides. The saturable decrease in signal was fit to the quadratic equilibrium binding eq 3 to obtain the K_D of interaction. In this equation, ΔF represents the change in fluorescence following each addition of the ACT from the initial fluorescence F_0 and ΔF_{MAX} represents the maximal change in fluorescence observed on saturation of AT.

$$\frac{\Delta F}{F_0} = \frac{\Delta F_{max}}{F_0} \times \{[([AT]_0 + [ACT]_0 + K_D) - \sqrt{([AT]_0 + [ACT]_0 + K_D)^2 - 4[AT]_0[ACT]_0}]/(2[AT]_0)\} \quad (3)$$

Factor Xa Inhibition Studies. The kinetics of inhibition of fXa by AT in the presence of the designed nonsaccharide aromatic activators was measured spectrophotometrically under pseudo-first-order conditions following our earlier work.[5,6,30,31] Briefly, a fixed concentration of fXa (20 nM) was incubated with fixed concentrations of plasma AT (1.075 μM) and sulfated activators (0−100 μM) in 20 mM sodium phosphate buffer, pH 6.0, containing 25 mM NaCl, 0.1 mM EDTA, and 0.1% (w/v) PEG8000 at 25 °C. At regular time intervals, an aliquot of the inhibition reaction was quenched with 900 μL of 100 μM Spectrozyme FXa in 20 mM sodium phosphate buffer, pH 7.4, containing 100 mM sodium chloride at 25 °C. To determine the residual fXa activity, the initial rate of substrate hydrolysis was measured from the increase in absorbance at 405 nm. The exponential decrease in the initial rate of substrate hydrolysis as a function of time was used to determine the observed pseudo-first-order rate constant of fXa inhibition (k_{OBS}). A plot of k_{OBS} at different concentrations of the activator could be described by eq 4, in which k_{UNCAT} is the second-order rate constant of fXa inhibition by AT alone and k_{ACT} is the second-order rate constant of fXa inhibition by AT−activator complex.

$$\frac{k_{OBS}}{[AT]_0} = k_{UNCAT} + k_{ACT} \times \frac{[ACT]_0}{[AT]_0 + K_D} \quad (4)$$

RESULTS AND DISCUSSION

Design Goals and Design Elements for Non-Heparin AT Activators. Figure 1A describes two possible mechanisms of AT activation process. The induced fit mechanism is followed by nearly all heparins, whereas the pre-equilibrium mechanism has been documented for oligosaccharides that lack the critical PBS recognition element.[5] The induced fit mechanism requires that the potential ligand recognize both the native (AT) as well as the activated state (AT*), while the pre-equilibrium mechanism primarily involves ligand recognition of AT* (Figure 1A). Despite considerable effort, the exact mechanism of how the activating conformational change is brought about through the induced fit process remains unclear. Thus design-wise, activators that utilize the pre-equilibrium pathway are expected to be easier to design as this pathway involves preferential recognition of only one AT form. Yet, an apparent limitation of the pre-equilibrium pathway could be inefficient activation because of the limiting rate of intrinsic conversion of AT to the AT* form. This implies that a key goal of the design strategy should be AT activation, which is reflected by the acceleration in the AT inhibition of fXa brought about by the designed activator. A secondary goal of the design strategy could be the affinity of the activator for AT. However, considering that the HBS of AT is a shallow, surface exposed region consisting primarily of amino acids involved in Coulomb-type interactions (Arg and Lys), high affinity as a "driver" of design could take lesser importance at this early stage of nonheparin, organic activator design.

Our first- and second-generation nonsaccharide heparin mimetics were found to bind in the EHBS and induce accelerated inhibition of fXa.[31,32] This suggested that the nonsaccharide AT activators most probably utilized the pre-equilibrium

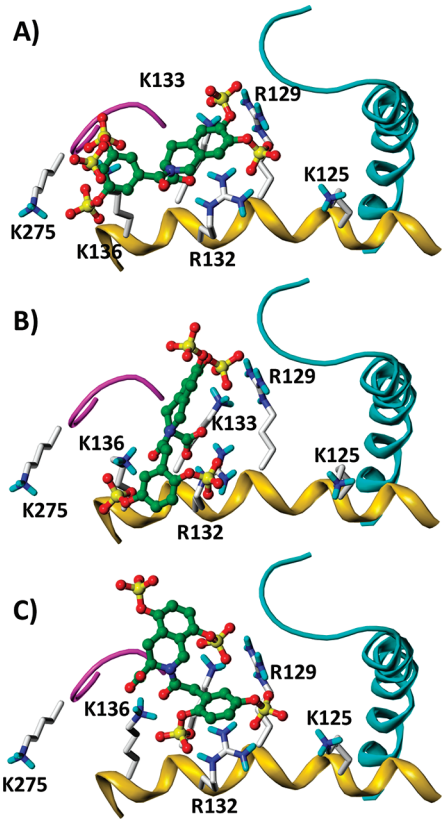

Figure 2. Computational screening of a library of 90 potential sulfated activators docked onto the extended heparin binding site of the activated form of AT using GOLD. Starting with IAS_5, our second-generation molecule showing 30-fold AT activation, a focused library considering structural variations on the positions of sulfate groups on the bicyclic and unicyclic rings, the presence or absence of carboxylic group at the 3-position, the stereochemistry at position 3, and the type of linker was built. Molecules showing high promise included **19a** and **20a** in both enantiomeric (*R* and *S*) forms. Shown here are three representative molecules. (A) (*S*)-IAS5, (B) (*S*)-**19a**, and (C) (*R*)-**20a**. See text for details.

mechanism. The fact that the pharmacophore-based design, IAS_5, could achieve ~30-fold acceleration in the inhibition of fXa suggested a strong potential of the pre-equilibrium mechanism, which was worth investigating further from the perspective of fundamental design principles.

Design of EHBS Targeting Potential AT Activators. To improve upon the AT activation potential achieved with IAS_5 by targeting the pre-equilibrium pathway of AT-mediated inhibition of fXa, a focused library of IAS_5-related THIQ derivatives was generated in silico. Combinations of five major structural variations were considered in developing the library. These included the positions of two sulfate groups on the bicyclic THIQ moiety (3 possibilities: 6,7-, 5,8-, and 5,6-), the presence or absence of carboxylic group at 3-position (2 possibilities: $-COO^-$ and $-H$), the stereochemistry of the carboxylate at the 3-position (2 possibilities: *R* and *S*), the amide linker extension (2 possibilities: 1-atom ($-CO-$) or 2-atom ($-CH_2-CO-$)), and finally the positions of either two or three sulfate groups on the monocyclic part (5 possibilities: 2,3-, 2,4-, 2,5-, 2,3,4-, and 3,4,5-sulfates).

The 90 designed potential sulfated activators were docked onto the EHBS of AT* using GOLD and scored using GOLD as well as HINT, as described earlier in our work.[30,32,37,40] In silico docking and scoring of highly sulfated molecules, e.g., those containing more than a couple of sulfate groups onto proteins, is still a growing area of algorithm design. There is no single algorithm that predicts binding site and geometry with high fidelity. Previously, we designed a combinatorial virtual library screening strategy to improve the predictability of complex geometry, however this strategy is finely tuned for heparin-like saccharide sequences, which display reduced flexibility around typical interglycosidic torsions.[37,41] Highly sulfated small organic molecules that exhibit significant backbone flexibility pose special challenges because of the phenomenally large conformational search space. The molecules tend to adopt multiple binding modes, which makes ranking less than straightforward. Hence, scoring with two functions, GOLD and HINT, was utilized.

The GOLD and HINT scores of our reference activator IAS_5 bound in the EHBS of AT* were 83.3 and 2200, respectively (Figure 2A). The activator was found to interact with Arg129, Arg132, and Lys136 of EHBS, which corroborates competitive studies performed earlier.[42] Analysis of the library docking results highlighted two molecules as potentially interesting, **19a** and **20a** (Figures 2B and 2C; chemical structures are in Scheme 2). The *S* isomers of **19a** and **20a** demonstrated GOLD scores of 83.9 and 93.0 and HINT scores of 2711 and 2772, respectively, while the *R* enantiomers had scores of 98.9 and 94.3 (GOLD) and 2200 and 2562 (HINT), respectively. This suggested that these designs may be potentially better at recognizing AT. The combinatorial library screen also indicated that 2,5-disulfated unicyclic ring was favored over four other possibilities and that both *R* and *S* enantiomers were likely to activate AT.

Molecules **19a** and **20a** were interesting from another angle too. These possess only four sulfate groups as opposed to five present in IAS_5. This aided our ultimate goal of designing activators with the minimum number of sulfate groups (probably three) on a small scaffold so as to eliminate nonspecific interactions arising from redundant negative charges. Reduced polyanionic character coupled with greater hydrophobicity of the scaffold may introduce oral bioavailability, a feature that nonsaccharide heparin mimetics are likely to possess.[32,34] Thus, we decided to develop a small group of molecules around the **19a** and **20a** structures to identify optimal sulfate positions on the THIQ moiety and study the effect of 3-carboxylic acid and unicyclic−bicyclic linker length on AT activation.

Synthesis of Non-Saccharide, Sulfated *N*-Arylacyl-THIQ Derivatives. Although THIQ is an important heterocyclic ring, synthesis of its derivatives with targeted substitutions described above is not well documented in the literature. Thus, much effort had to be directed toward establishing a high yield protocol for 3-carboxylic acid derivatives of THIQ, referred to as THIQ3CA. Traditional methods such as Pictet−Spengler,[43] Bischler−Napieralski,[44] and Pomeranz−Fritsch[45] reactions could not be readily adapted to our synthesis because of the limited availability of the required starting materials. Therefore, the THIQ3CA scaffold was constructed from three components, formaldehyde, substituted benzaldehyde, and glycine moiety donor, in four steps (Scheme 2). In our synthetic design, *N*-Boc-α-phosphonoglycine trimethylester served as the glycine donor. Briefly, the Horner−Wadsworth−Emmons reaction of the glycine donor and the desired dimethoxy benzaldehyde **9** or **10** afforded the corresponding benzylidene in excellent yields. This was followed by catalytic hydrogenation using palladized charcoal, *N*-Boc deprotection using acidic conditions, and Pictet−Spengler

Scheme 1[a]

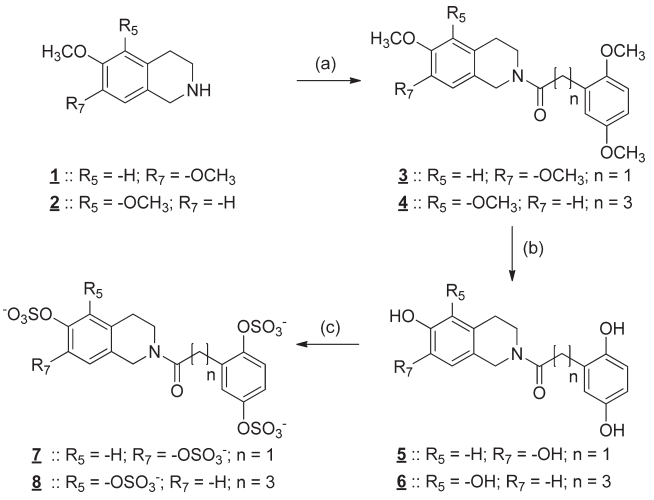

[a] (a) 2,5-Dimethoxyphenyl acetic ($n = 1$) or butanoic acid ($n = 3$), EDCI, DMAP, rt/overnight, 70−95%; (b) BBr_3/CH_2Cl_2, −78 °C/2 h, then rt/overnight, 65−85%; (c) SO_3:NMe_3/(1:1) DMF:CH_3CN, 80 °C/5 h, followed by Na^+ exchange 45−75%.

cyclization with formaldehyde to give THIQ3CA methyl esters **13** and **14** in approximately 55% overall yield. Noncarboxylated THIQ derivative **2** was obtained through direct application of Pictet−Spengler reaction on the corresponding substituted phenethylamine (Scheme 1) while 6,7-dimethoxy THIQ, **1**, is commercially available.

The THIQ3CA esters were then elaborated to the bicyclic−unicyclic structures with variable linkers by coupling with appropriately substituted arylalkyl carboxylic acids. Thus, coupling with 2-(2,5-dimethoxy phenyl)acetic acid afforded the *N*-arylacylated THIQ3CA esters with a 2-atom linker (**15a**, **16a**), whereas 3-atom (**15b**, **16b**) and 4-atom linker structures (**15c**, **16c**) were prepared using propionic and butanoic acid derivatives, respectively. The methoxy protecting groups of the coupled *N*-arylacylated THIQ3CA esters were then removed using BBr_3 in CH_2Cl_2, which also led to the concomitant hydrolysis of the carboxylic ester, to yield the per-phenolic *N*-arylacyl THIQ3CAs (**17a**−**17c**, **18a**−**18c**). Likewise, the noncarboxylated THIQ derivatives, **3** and **4**, as well as the corresponding per-phenolic THIQs, **5** and **6**, were generated in a similar manner. Overall, the synthesis of the per-phenolic precursors of AT activators from the THIQ scaffold was achieved in 65−85% yield. To the best of our knowledge, these THIQ derivatives have not been reported in the literature and these high yields appear to be the best achieved so far for this class of molecules.

The conversion of per-phenolic precursors, such as **17a**−**17c** and **18a**−**18c**, to their per-sulfated derivatives is known to be a challenging.[46,47] We have earlier developed a base-mediated, microwave-assisted per-sulfation protocol,[46] however, this method resulted in partially sulfated compounds as well as degradation products as demonstrated by CE analysis. We inferred that the free carboxylic group of **17a**−**17c** and **18a**−**18c** interferes with base-mediated persulfation and hence explored neutral conditions without microwave heating. Refluxing the per-phenolic precursors in a 1:1 mixture of CH_3CN:DMF with Me_3N:SO_3 complex for 5 h gave significantly improved yields (41−75%) of the per-sulfated products (**7**, **8**, **19a**−**19c**, **20a**−**20c**) (Schemes 1 and 2). It is worth mentioning here that per-sulfation of at least 12 phenolic THIQs was attempted, however, only eight compounds could be successfully isolated. Derivatives with 5,6-disulfate and 3-carboxylate groups proved to be the most difficult perhaps because of limited access to the 5-position.

Affinity of Sulfated *N*-arylacyl-THIQ Activators for Antithrombin. The binding affinity of heparins for plasma AT is typically measured through the 30−40% increase in intrinsic tryptophan fluorescence as a function of the concentration of the activator.[4−6] However, this technique did not work with our first-generation nonsaccharide activators because of insufficient signal.[30,32] Later work with second-generation molecules demonstrated a significantly different signal in comparison to the heparins. For IAS_5-based activators, the intrinsic fluorescence decreased and reached a plateau at high ligand concentrations.[31] We used this approach to measure the K_D for AT interaction with the per-sulfated activators (**7**, **8**, **19a**−**19c**, **20a**−**20c**) in 20 mM sodium phosphate buffer, pH 6.0. Increasing concentrations of the synthesized per-sulfated derivatives gave a saturable decrease in intrinsic fluorescence of AT (Figure 3). The maximal change in fluorescence (ΔF_{MAX}) was found to be in the range of 25−100%, which provided excellent signal for K_D measurement. For each per-sulfated derivative, the observed fluorescence decrease was fitted by the standard quadratic binding eq 3 to calculate the K_D of AT−activator complex (Table 1).

Overall, the AT affinity of the THIQ-based focused library was found to be mediocre to poor (80−3900 μM) in comparison to DEFGH (~0.001 μM).[5] This is not too surprising considering that the DEFGH sequence has been optimized by nature through millions of years of evolution and heparin seems to have been designed specifically for recognizing AT. With regard to our first- and second-generation activators (2−300 μM), the measured affinity of activators studied in this work is less than expected.[30,31] An important reason for this weaker affinity is that ECS and IAS_5 (Figure 1B) relied on a much smaller scaffold, which increases the sulfate charge density with a concomitant rise in the Coulombic forces of attraction.[47]

Despite the relatively weak interaction with AT, the affinities demonstrate a strong structural dependence. For the 5,8-series containing the carboxylic acid group, the AT binding affinity ranged from 394 μM for **20a**, containing a 2-atom linker, to 1322 μM for **20c**, containing a 4-atom linker (Table 1). Likewise, the AT affinity for the carboxylated 6,7-series ranged from 81 μM for **19a**, containing the 2-atom linker, to 3883 μM for **19c**, containing the 4-atom linker. Last, activators **7** and **8**, lacking 3-carboxylic acid group, demonstrated K_D of 753 and 1123 μM, respectively. The nonlinear variation in affinity of these activators, more clearly demonstrated in the 6,7 series, probably suggests significant differences in binding mode despite their relatively similar structures.

Antithrombin Activation by Sulfated *N*-arylacyl THIQ Derivatives. A characteristic of AT activation is the acceleration in the rate of fXa inhibition by heparins and heparin mimetics. Accordingly, the second-order rate constant of AT inhibition of fXa in presence (k_{ACT}) and absence (k_{UNCAT}) of sulfated *N*-arylacyl-THIQ derivatives was measured at pH 6.0, 25 mM NaCl, and 25 °C, as described earlier in our previous work.[5,6,31] In this technique, the residual fXa activity is measured at various time intervals at a fixed concentration of the activator to determine the pseudo-first-order observed rate constant (k_{OBS}). Several k_{OBS} measurements at various

Scheme 2[a]

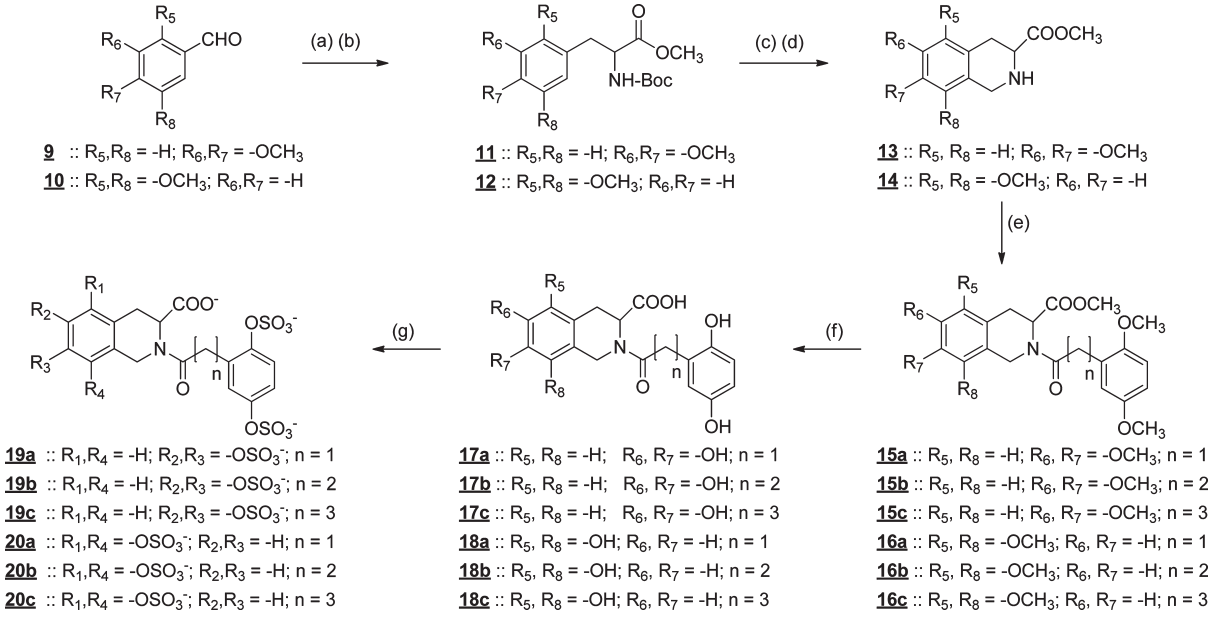

[a] (±)-Boc-α-phosphonoglycine trimethylester, DBU/THF, rt/overnight, 77−85%; (b) H_2/Pd/ethanol, rt/5 h, 100%; (c) (1:1) TFA:CH_2Cl_2, rt/4 h, 85%; (d) 37% HCHO/TFA/CH_2Cl_2, rt/5 h, 70−80%; (e) 2,5-dimethoxyphenyl acetic (n = 1), propionic (n = 2), or butanoic acid (n = 3), EDCI, DMAP, rt/overnight, 70−95%; (f) BBr_3/CH_2Cl_2, −78 °C/2 h, then rt/overnight, 65−85%;, (g) SO_3:NMe_3/(1:1) DMF:CH_3CN, 80 °C/5 h, followed by Na^+ exchange 45−75%.

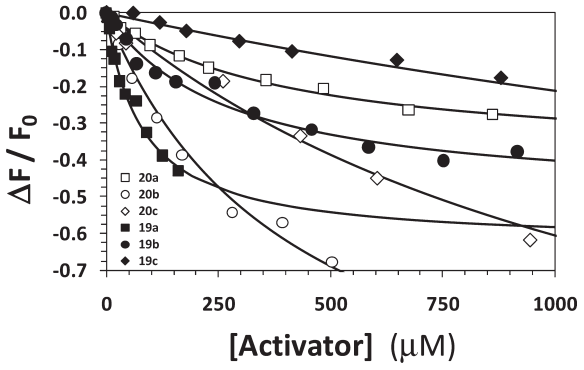

Figure 3. Spectrofluorimetric measurement of the AT affinity of sulfated *N*-arylacyl-THIQ activators at pH 6.0, *I* 0.05, 25 °C. The binding of the activators (○ = **20b**; □ = **20a**; ◇ = **20c**; ◆ = **19c**; ● = **19b**; ■ = **19a**) to AT resulted in a saturable decrease in intrinsic tryptophan fluorescence at 340 nm (λ_{EX} = 280 nm), which was fitted to the quadratic binding eq 3 to calculate the observed K_D. Solid lines represent the nonlinear regressional fit.

Table 1. Antithrombin Affinity of Sulfated Tetrahydroisoquinoline Activators[a]

activator	K_D (μM)	ΔF_{MAX} (%)
7	753 ± 478[b]	−38 ± 14
8	1123 ± 191	−24 ± 2
19a	81 ± 14	−63 ± 5
19b	273 ± 49	−51 ± 4
19c	3883 ± 1325	−104 ± 26
20a	394 ± 46	−40 ± 2
20b	420 ± 38	−127 ± 8
20c	1322 ± 237	−140 ± 14
IAS_5[c]	320 ± 10	−130 ± 20
ECS[d]	10.5 ± 1.2	na[e]

[a] Affinity was measured using the decrease in intrinsic tryptophan fluorescence as a function of activator concentration in 20 mM sodium phosphate buffer, pH 6.0, containing 25 mM sodium chloride, 0.1 mM EDTA, and 0.1% PEG 8000 at 25 °C. See Experimental Section for additional details. [b] Error represents ±1 SE. [c] Taken from ref 31. [d] Taken from ref 32 and corresponds to results measured in 20 mM sodium phosphate buffer, pH 6.0, containing 0.1 mM EDTA and 0.1% PEG8000. [e] Not applicable.

concentrations of the activator are performed to assess the phenomenon of AT activation. Figure 4 shows representative profiles for **19a** and **20b** in the concentration ranges of 0 → 9 μM and 0 → 28 μM, respectively. At a qualitative level, the profiles suggest that **19a** (Figure 4A) accelerates AT inhibition of fXa at a rate faster than **20b** (Figure 4B).

To evaluate AT activation on a quantitative level, the increase in k_{OBS} as a function of the concentration of the each activator was analyzed using eq 4, as described earlier.[31] The slope of this plot provides the second-order rate constant of fXa inhibition by AT−activator complex (k_{ACT}), while the intercept yields the second-order rate constant of fXa inhibition by AT alone (k_{UNCAT}). The ratio of k_{ACT} to k_{UNCAT} provides the acceleration in AT inhibition of fXa, a measure of AT activation induced by the activator. Figure 5 shows the profiles measured for each *N*-arylacyl-THIQ activator, and Table 2 lists the acceleration calculated from the linear fits to the data. The data indicate significant differences in the acceleration potential of each sulfated activator.

The AT acceleration potential was found to be 79.4 for **20c**, 29.3 for **20b**, and 67.1 for **20a**, while it was 23.7 for **19c**, 16.5 for **19b**, and 53.2 for **19c** under identical conditions (pH 6.0, 25 mM NaCl, 25 °C). These results put forward three molecules studied

dx.doi.org/10.1021/jm2008387 |*J. Med. Chem.* 2011, 54, 6125–6138

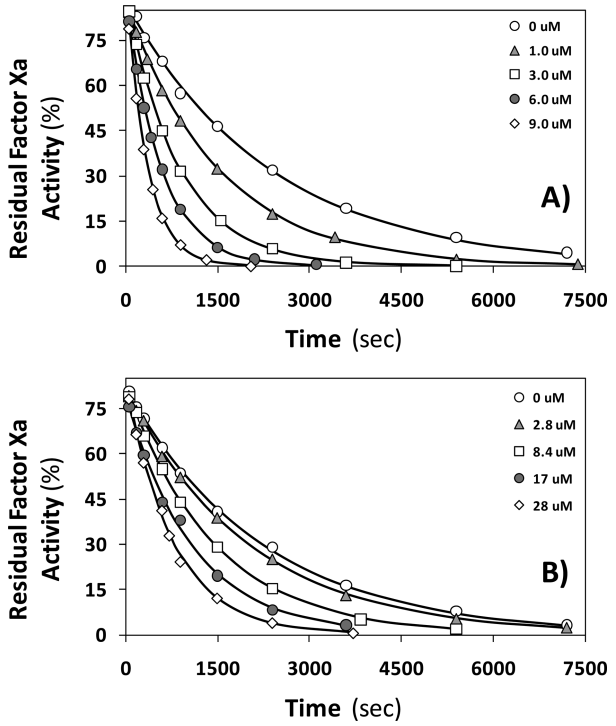

Figure 4. Kinetics of antithrombin inhibition of factor Xa in the presence of sulfated *N*-arylacyl-tetrahydroisoquinoline activators **19a** (A) and **20b** (B) at pH 6.0, *I* 0.05, 25 °C. The residual fXa activity was measured spectrophotometrically under pseudo-first-order conditions through the initial rate of Spectrozyme FXa hydrolysis. The observed pseudo-first-order rate constant of fXa inhibition (k_{OBS}) at each activator concentration was calculated from the exponential decrease. See Experimental Section for details.

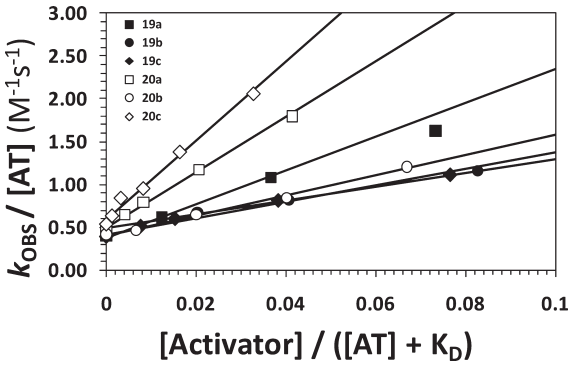

Figure 5. Acceleration in factor Xa inhibition by antithrombin-sulfated *N*-arylacyl-tetrahydroisoquinoline activator complexes. The observed rate constant (k_{OBS}) of fXa inhibition by AT in the presence of varying concentrations of the activator (○ = **20b**; □ = **20a**; ◇ = **20c**; ◆ = **19c**; ● = **19b**; ■ = **19a**) was measured in a spectrophotometric assay at pH 6.0, *I* 0.05, and 25 °C. Solid lines represent linear regressional fits to the data using eq 4 to calculate the second-order rate constants, k_{ACT} and k_{UNCAT}. See text for details.

here as significantly better than the best nonsaccharide aromatic AT activator designed earlier.[31] Specifically, **20c**, **20a**, and **19a** accelerate AT inhibition of fXa much better than IAS_S. More importantly, the acceleration induced by **20c**, i.e., 79-fold, is only 3.8-fold lower than the 300-fold acceleration induced by DEFGH. In terms of advance in activator design, **20c** displays nearly 10-fold higher AT activation potential than the first designed nonsaccharide aromatic activator.[30]

Table 2. Acceleration in Antithrombin Inhibition of Factor Xa by Sulfated Tetrahydroisoquinoline Activators[a]

activator	k_{UNCAT} (M^{-1} s^{-1})	k_{ACT} (M^{-1} s^{-1})	acceleration
7	386 ± 27[b]	4582 ± 597	11.0 ± 2.2
8	375 ± 22	3337 ± 265	8.3 ± 1.1
19a	345 ± 38	19740 ± 1290	53.2 ± 9.3
19b	454 ± 21	8051 ± 751	16.5 ± 2.3
19c	378 ± 15	9640 ± 748	23.7 ± 2.8
20a	452 ± 17	32630 ± 1644	67.1 ± 5.9
20b	374 ± 10	11800 ± 789	29.3 ± 2.8
20c	543 ± 28	46330 ± 2830	79.4 ± 8.9
IAS_S[c]	~2300	69780 ± 580	~30.3
ECS[d]	~120	909 ± 40	~7.6

[a] Antithrombin activation was measured using the a discontinuous slow kinetics assay of monitoring residual fXa following incubation in the presence of the activator at a fixed concentration in 20 mM sodium phosphate buffer, pH 6.0, containing 25 mM sodium chloride, 0.1 mM EDTA, and 0.1% PEG 8000 at 25 °C. See Experimental Section for details. [b] Error represents ±1 SE. [c] Taken from ref 31 and corresponds to results measured in 20 mM sodium phosphate buffer, pH 7.4, containing 100 mM NaCl, 0.1 mM EDTA and 0.1% PEG8000. [d] Taken from ref 32 and corresponds to results measured in 20 mM sodium phosphate buffer, pH 6.0, containing 0.1 mM EDTA and 0.1% PEG8000.

The results also indicate that the 5,8 series of activators is better than the 6,7 series of activators. Yet, the AT activation potential appears to follow a nonlinear pattern with regard to the length of the linker in both series of molecules. For example, the 3-atom linker containing activator in both the series (5,8- and 6,7-series) displays weaker acceleration than the 2- and 4-atom counterparts. The reason for this behavior is not clear but may be due to different mode of binding of each activator. Finally, derivatives **7** and **8**, which lack the 3-carboxylic acid group on the THIQ ring, exhibited AT acceleration of only 11 ± 2.2 and 8.3 ± 1.1, respectively. This implies that 3-carboxylic acid functionality of these activators is important for activation of AT.

Finally, to assess the importance of sulfate groups in these activators, several per-phenolic parents of the sulfated activators were evaluated for interaction with AT and fXa. None of the tested per-phenolic parents displayed any measurable interaction (data not shown). Further, each sulfated activator was assessed for its direct interaction with fXa in the absence of AT and found to lack of any direct inhibition effect (data not shown). These results support the conclusion that the designed bicyclic-unicyclic sulfated *N*-arylacyl THIQ derivatives function as indirect inhibitors of fXa through allosteric activation of AT.

■ CONCLUSIONS AND SIGNIFICANCE

Heparins form one of the two major classes of anticoagulant drugs in use today. Although heparin-based therapy is continuously advancing, the advancements in terms of medicinal chemistry have not led to structures beyond the heparin pentasaccharide. Fundamental research is necessary for scaffold hopping so as to derive clinically viable candidates. Yet, scaffold hopping is challenging, as demonstrated by our earlier

work[30−34] as well as by recent efforts from the Pinto group,[48,49] both of which indicate relatively weak affinity of the designed molecules.

Despite this difficulty, our molecular docking and scoring protocol indicates a reasonable level of success. Molecules identified through virtual screening, **19a** and **20a** showed K_D of 81 and 394 μM, respectively, while their AT acceleration potentials were 53- and 67-fold, respectively. These results indicate significant improvements over our second-generation AT activator IAS_5. Our work highlights a critical aspect of allosteric conformational activation of AT. Whereas the affinity of the third-generation activators studied in this work was lower than that studied in our earlier work,[30,31] the activation potential measured was found to be higher. This shows a segregation of affinity and activation potential, as expected on the basis of the theory of two-step allosteric activation. Affinity reflects the strength with which an activator binds in the EHBS, whereas activation potential is a measure of the stability of the conformational change induced in AT. This work shows that **19a** and **20a** although not fitting perfectly in the EHBS are able to induce sufficient conformational change in AT to inhibit factor Xa at a higher rate. Because our analysis evaluates the properties of the AT−activator complex (i.e., under saturation), we are able to parse affinity and activation parameters, which provides a unique insight into the mechanism of allosteric activation. Yet, detailed mechanistic and structural biology studies are necessary to ascertain whether the new molecules bind in the EHBS. Overall, the results support the concept that targeting the pre-equilibrium pathway and the EHBS may be viable route to new AT activators.

An important point that our study affords is the correlation of GOLD and HINT scores with affinity measured for the series of sulfated *N*-arylacyl tetrahydroisoquinoline derivatives. A qualitative correlation was evident from this limited study, but upon detailed quantitative evaluation, the correlation is not strong. Molecular modeling studies of highly sulfated carbohydrates and noncarbohydrates have also been challenging,[30,32,37,40,50] especially because appropriate docking and scoring tools have not been developed for sulfated molecules as they have been for traditional hydrophobic small molecules. Yet, sulfated *N*-arylacyl tetrahydroisoquinolines appear to have an added complication. These molecules display conformational isomerism, as evident from the NMR studies reported above, which raises the possibility of complications arising from selectivity of recognition.

The best molecule in the series studied here, i.e., **20c**, is only 3.8-fold less efficient at AT activation than the "gold" standard, DEFGH. This is a considerable advance. However, this does not imply that the design of a clinically viable nonsaccharide AT activator is within rapid reach. One, the potency of **20c** is inadequate. We estimate that an AT affinity at least four orders of magnitude higher will be needed for clinical viability. This may appear to be a tall order, but subtle changes in design may engineer a nearly impeccable structural fit to EHBS residues. Two, an AT activation higher than the 80-fold achieved **20c** may be necessary. This does not imply that 300-fold activation, as for the "gold" standard DEFGH, is an absolute necessity for clinical viability. The important parameter that will govern clinical relevance is likely to be activation to toxicity ratio, which should favor activation by a high margin. In this regard, toxicity studies with liver HepG2 and lung A549 cells lines show minimal toxicity of these types of highly water-soluble molecules at levels as high as 50 mg/L (data not presented). This implies that activation less than 300-fold may not be a major limitation.

We expect **20c** to serve as an excellent scaffold for further design modifications. A specific advantage of these nonsaccharide AT activators is that their synthesis is much simpler than the heparin-based activators.[10] This implies that a library of diverse analogues around the **20c** scaffold can be prepared without much difficulty to identify more potent and efficacious molecules. This work is in progress.

AUTHOR INFORMATION

Corresponding Author

*Phone: 804-828-7328. Fax: 804-827-3664. E-mail: urdesai@vcu.edu. Address: Department of Medicinal Chemistry, Virginia Commonwealth University, 800 East Leigh Street, Suite 212, P.O. Box 980133, Richmond, VA 23219.

ACKNOWLEDGMENT

This work was supported by grants HL099420 and HL090586 from the National Institutes of Health. We thank Dr. Philip Mosier for help with molecular modeling and preparation of Figure 2.

ABBREVIATIONS USED

AT, antithrombin; CE, capillary electrophoresis; EHBS, extended heparin-binding site; FLH, full-length heparin; fXa, factor Xa; H, heparin; HBS, heparin-binding site; I, ionic strength; LMWH, low-molecular-weight heparin; PBS, pentasaccharide-binding site; THIQ, tetrahydroisoquinoline; THIQ3CA, tetrahydoisoquinoline-3-carboxylic acid

REFERENCES

(1) Björk, I.; Olson, S. T. Antithrombin. A bloody important serpin. *Adv. Exp. Med. Biol.* **1997**, *425*, 17–33.

(2) Desai, U. R. New antithrombin-based anticoagulants. *Med. Res. Rev.* **2004**, *24*, 151–181.

(3) Olson, S. T.; Swanson, R.; Raub-Segall, E.; Bedsted, T.; Sadri, M.; Petitou, M.; Herault, J. P.; Herbert, J. M.; Björk, I. Accelerating ability of synthetic oligosaccharides on antithrombin inhibition of proteinases of the clotting and fibrinolytic systems. Comparison with heparin and low-molecular-weight heparin. *Thromb. Haemostasis* **2004**, *92*, 929–939.

(4) Olson, S. T.; Björk, I.; Sheffer, R.; Craig, P. A.; Shore, J. D.; Choay, J. Role of the antithrombin-binding pentasaccharide in heparin acceleration of antithrombin proteinase reactions. Resolution of the antithrombin conformational change contribution to heparin rate enhancement. *J. Biol. Chem.* **1992**, *267*, 12528–12538.

(5) Desai, U. R.; Petitou, M.; Björk, I.; Olson, S. T. Mechanism of heparin activation of antithrombin: role of individual residues of the pentasaccharide activating sequence in the recognition of native and activated states of antithrombin. *J. Biol. Chem.* **1998**, *273*, 7478–7487.

(6) Desai, U. R.; Petitou, M.; Björk, I.; Olson, S. T. Mechanism of heparin activation of antithrombin: evidence for an induced fit model of allosteric activation involving two interaction subsites. *Biochemistry* **1998**, *37*, 13033–13041.

(7) Jin, L.; Abrahams, J.-P.; Skinner, R.; Petitou, M.; Pike, R. N.; Carrell, R. W. The anticoagulant activation of antithrombin by heparin. *Proc. Natl. Acad. Sci. U.S.A.* **1997**, *94*, 14683–14688.

(8) Arocas, V.; Turk, B.; Bock, S. C.; Olson, S. T.; Björk, I. The region of antithrombin interacting with full-length heparin chains outside the high-affinity pentasaccharide sequence extends to Lys136 but not to Lys139. *Biochemistry* **2000**, *39*, 8512–8518.

(9) Petitou, M.; Barzu, T.; Herault, J. P.; Herbert, J. M. A unique trisaccharide sequence in heparin mediates the early step of antithrombin III activation. *Glycobiology* **1997**, *7*, 323–327.

(10) Petitou, M.; van Boeckel, C. A. A synthetic antithrombin III binding pentasaccharide is now a drug! What comes next? *Angew. Chem., Int. Ed. Engl.* **2004**, *43*, 3118–3133.

(11) Hirsh, J.; Anand, S. S.; Halperin, J. L.; Fuster, V. Guide to anticoagulant therapy: heparin. *Circulation* **2001**, *103*, 2994–3018.

(12) Blossom, D. B.; Kallen, A. J.; Patel, P. R.; Elward, A.; Robinson, L.; Gao, G.; Langer, R.; Perkins, K. M.; Jaeger, J. L.; Kurkjian, K. M.; Jones, M.; Schillie, S. F.; Shehab, N.; Ketterer, D.; Venkataraman, G.; Kishimoto, T. K.; Shriver, Z.; McMahon, A. W.; Austen, K. F.; Kozlowski, S.; Srinivasan, A.; Turabelidze, G.; Gould, C. V.; Arduino, M. J.; Sasisekharan, R. Outbreak of adverse reactions associated with contaminated heparin. *N. Engl. J. Med.* **2008**, *359*, 2674–2684.

(13) Guerrini, M.; Beccati, D.; Shriver, Z.; Naggi, A.; Viswanathan, K.; Bisio, A.; Capila, I.; Lansing, J. C.; Guglieri, S.; Fraser, B.; Al-Hakim, A.; Gunay, N. S.; Zhang, Z.; Robinson, L.; Buhse, L.; Nasr, M.; Woodcock, J.; Langer, R.; Venkataraman, G.; Linhardt, R. J.; Casu, B.; Torri, G.; Sasisekharan, R. Oversulfated chondroitin sulfate is a contaminant in heparin associated with adverse clinical events. *Nature Biotechnol.* **2008**, *26*, 669–675.

(14) Kishimoto, T. K.; Viswanathan, K.; Ganguly, T.; Elankumaran, S.; Smith, S.; Pelzer, K.; Lansing, J. C.; Sriranganathan, N.; Zhao, G.; Galcheva-Gargova, Z.; Al-Hakim, A.; Bailey, G. S.; Fraser, B.; Roy, S.; Rogers-Cotrone, T.; Buhse, L.; Whary, M.; Fox, J.; Nasr, M.; Dal Pan, G. J.; Shriver, Z.; Langer, R. S.; Venkataraman, G.; Austen, K. F.; Woodcock, J.; Sasisekharan, R. Contaminated heparin associated with adverse clinical events and activation of the contact system. *N. Engl. J. Med.* **2008**, *358*, 2457–2467.

(15) Gray, E.; Mulloy, B.; Barrowcliffe, T. W. Heparin and low-molecular-weight heparin. *Thromb. Haemostasis* **2008**, *99*, 807–818.

(16) Rabenstein, D. L. Heparin and heparin sulfate: structure and function. *Nat. Prod. Rep.* **2002**, *19*, 312–331.

(17) Tran, A. H.; Lee, G. Fondaparinux for prevention of venous thromboembolism in major orthopedic surgery. *Ann. Pharmacother.* **2003**, *37*, 1632–1643.

(18) Tsiridis, E.; Gamie, Z.; George, M. J.; Hamilton-Baille, D.; West, R. M.; Giannoudis, P. V. Early postoperative bleeding in polytrauma patients treated with fondaparinux: literature review and institutional experience. *Curr. Vasc. Pharmacol.* **2011**, *9*, 42–47.

(19) Akl, E. A.; Vasireddi, S. R.; Gunukula, S.; Barba, M.; Sperati, F.; Terrenato, I.; Muti, P.; Schünemann, H. Anticoagulation for the initial treatment of venous thromboembolism in patients with cancer. *Cochrane Database Syst. Rev.* **2011**, *6*, CD006649.

(20) Brito, V.; Ciapponi, A.; Kwong, J. Factor Xa inhibitors for acute coronary syndromes. *Cochrane Database Syst Rev.* **2011**, *1*, CD007038.

(21) Minix, R.; Doctor, V. Interaction of fucoidan with proteases and inhibitors of coagulation and fibrinolysis. *Thromb. Res.* **1997**, *87*, 419–429.

(22) Pereira, M. S.; Mulloy, B.; Mourao, P. A. S. Structure and anticoagulant activity of sulfated fucans: comparison between the regular, repetitive, and linear fucans from echniderms with the more heterogeneous and branched polymers from brown algae. *J. Biol. Chem.* **1999**, *274*, 7656–7667.

(23) Alban, S.; Franz, G. Characterization of the anticoagulant actions of a semisynthetic Curdlan sulfate. *Thromb. Res.* **2000**, *99*, 377–388.

(24) Drozd, N. N.; Sher, A. I.; Makarov, V. A.; Galbraikh, L. S.; Vikhoreva, G. A.; Gorbachiova, I. N. Comparison of antithrombin activity of the polysulphate chitosan derivatives in in vivo and in vitro system. *Thromb. Res.* **2001**, *102*, 445–455.

(25) Pires, L.; Gorin, P. A. J.; Reicher, F.; Sierakowski, M.-R. An active heparinoid obtained by sulphation of a galactomannan extracted from the endosperm of *Senna macranthera* seeds. *Carbohydr. Polym.* **2001**, *46*, 165–169.

(26) Majdoub, H.; Ben Mansour, M.; Chaubet, F.; Roudesli, M. S.; Maaroufi, R. M. Anticoagulant activity of a sulfated polysaccharide from the green alga *Arthrospira platensis*. *Biochim. Biophys. Acta* **2009**, *1790*, 1377–1381.

(27) Pawlaczyk, I.; Czerchawski, L.; Kuliczkowski, W.; Karolko, B.; Pilecki, W.; Witkiewicz, W.; Gancarz, R. Anticoagulant and anti-platelet activity of polyphenolic-polysaccharide preparation isolated from the medicinal plant *Erigeron canadensis* L. *Thromb. Res.* **2011**, *127*, 328–340.

(28) de Kort, M.; Buijsman, R. C.; van Boeckel, C. A. Synthetic heparin derivatives as new anticoagulant drugs. *Drug Discovery Today* **2005**, *10*, 769–779.

(29) Avci, F. Y.; Karst, N. A.; Linhardt, R. J. Synthetic oligosaccharides as heparin-mimetics displaying anticoagulant properties. *Curr. Pharm. Des.* **2003**, *9*, 2323–2335.

(30) Gunnarsson, G. T.; Desai, U. R. Designing small, non-sugar activators of antithrombin using hydropathic interaction analyses. *J. Med. Chem.* **2002**, *45*, 1233–1243.

(31) Raghuraman, A.; Liang, A.; Krishnasamy, C.; Lauck, T.; Gunnarsson, C. T.; Desai, U. R. On designing non-saccharide, allosteric activators of antithrombin. *Eur. J. Med. Chem.* **2009**, *44*, 2626–2631.

(32) Gunnarsson, G. T.; Desai, U. R. Interaction of sulfated flavanoids with antithrombin: Lessons on the design of organic activators. *J. Med. Chem.* **2002**, *45*, 4460–4470.

(33) Gunnarsson, G. T.; Desai, U. R. Exploring new non-sugar sulfated molecules as activators of antithrombin. *Bioorg. Med. Chem. Lett.* **2003**, *13*, 579–583.

(34) Liang, A.; Thakkar, J. N.; Desai, U. R. Study of physicochemical properties of novel highly sulfated, aromatic, mimetics of heparin and heparan sulfate. *J. Pharm. Sci.* **2010**, *99*, 1207–1216.

(35) Freeman, C.; Liu, L.; Banwell, M. G.; Brown, K. J.; Bezos, A.; Ferro, V.; Parish, C. R. Use of sulfated linked cyclitols as heparan sulfate mimetics to probe the heparin/heparan sulfate binding specificity of proteins. *J. Biol. Chem.* **2005**, *280*, 8842–8849.

(36) Kim, S. K.; Huh, J.; Kim, S. Y.; Byun, Y.; Lee, D. Y.; Moon, H. T. Physicochemical conjugation with deoxycholic acid and dimethylsulfoxide for heparin oral delivery. *Bioconjugate Chem.* **2011**, *22*, 1451–1458.

(37) Raghuraman, A.; Mosier, P. D.; Desai, U. R. Finding a needle in a haystack. Development of a combinatorial virtual screening approach for identifying high specificity heparin/heparan sulfate sequence(s). *J. Med. Chem.* **2006**, *49*, 3553–3562.

(38) Kellogg, G. E.; Abraham, D. J. Hydrophobicity: is LogP(o/w) more than the sum of its parts? *Eur. J. Med. Chem.* **2000**, *35*, 651–661.

(39) Tripathi, A.; Surface, J. A.; Kellogg, G. E. Using active site mapping and receptor-based pharmacophore tools: prelude to docking and de novo/fragment-based ligand design. *Methods Mol. Biol.* **2011**, *716*, 39–54.

(40) Gunnarsson, G. T.; Desai, U. R. Hydropathic interaction analyses of small organic activators binding to antithrombin. *Bioorg. Med. Chem.* **2004**, *12*, 633–640.

(41) Raghuraman, A.; Mosier, P. D.; Desai, U. R. Understanding dermatan sulfate−heparin cofactor II interaction through virtual library screening. *ACS Med. Chem. Lett.* **2010**, *1*, 281–285.

(42) Liang, A.; Raghuraman, A.; Desai, U. R. Capillary electrophoretic study of small, highly sulfated, non-sugar molecules interacting with antithrombin. *Electrophoresis* **2009**, *30*, 1544–1551.

(43) Cox, E. D.; Cook, J. M. The Pictet−Spengler condensation: a new direction for an old reaction. *Chem. Rev.* **1995**, *95*, 1797–1842.

(44) Whaley, W. M.; Govindachari, T. R. Preparation of 3,4-dihydroisquinolines and related compounds by the Bischler−Napieralski reaction. *Org. React.* **1951**, *6*, 74–150.

(45) Chrzanowska, M.; Rozwadowska, M. D. Asymmetric synthesis of isoquinoline alkaloids. *Chem. Rev.* **2004**, *104*, 3341–3370.

(46) Raghuraman, A.; Riaz, M.; Hindle, M.; Desai, U. R. Rapid, high-yielding microwave-assisted per-sulfation of organic scaffolds. *Tetrahedron Lett.* **2007**, *48*, 6754–6758.

(47) Al-Horani, R. A.; Desai, U. R. Chemical sulfation of small molecules—advances and challenges. *Tetrahedron* **2010**, *66*, 2907–2918.

(48) Correia-da-Silva, M.; Sousa, E.; Duarte, B.; Marques, F.; Carvalho, F.; Cunha-Ribeiro, L. M.; Pinto, M. M. Flavonoids with an oligopolysulfated moiety: A new class of anticoagulant agents. *J. Med. Chem.* **2011**, *54*, 95–106.

(49) Correia-da-Silva, M.; Sousa, E.; Duarte, B.; Marques, F.; Cunha-Ribeiro, L. M.; Pinto, M. M. Dual anticoagulant/antiplatelet persulfated small molecules. *Eur. J. Med. Chem.* **2011**, *46*, 2347–2358.

(50) Grootenhuis, P. D. J.; van Boeckel, C. A. A. Constructing a molecular model of the interaction between antithrombin III and a potent heparin analogue. *J. Am. Chem. Soc.* **1991**, *113*, 2743–2747.